Biochemistry

pubs.acs.org/biochemistry Article

Insights into Cerebral Amyloid Angiopathy Type 1 and Type 2 from Comparisons of the Fibrillar Assembly and Stability of the Aβ40-Iowa and Aβ40-Dutch Peptides

Jitika Rajpoot, Elliot J. Crooks, Brandon A. Irizarry, Ashley Amundson, William E. Van Nostrand, and Steven O. Smith*

Cite This: *Biochemistry* 2022, 61, 1181−1198 Read Online

ACCESS | Metrics & More | Article Recommendations | Supporting Information

ABSTRACT: Two distinct diseases are associated with the deposition of fibrillar amyloid-β (Aβ) peptides in the human brain in an age-dependent fashion. Alzheimer's disease is primarily associated with parenchymal plaque deposition of Aβ42, while cerebral amyloid angiopathy (CAA) is associated with amyloid formation of predominantly Aβ40 in the cerebral vasculature. In addition, familial mutations at positions 22 and 23 of the Aβ sequence can enhance vascular deposition in the two major subtypes of CAA. The E22Q (Dutch) mutation is associated with CAA type 2, while the D23N (Iowa) mutation is associated with CAA type 1. Here we investigate differences in the formation and structure of fibrils of these mutant Aβ peptides *in vitro* to gain insights into their biochemical and physiological differences in the brain. Using Fourier transform infrared and nuclear magnetic resonance spectroscopy, we measure the relative propensities of Aβ40-Dutch and Aβ40-Iowa to form antiparallel structure and compare these propensities to those of the wild-type Aβ40 and Aβ42 isoforms. We find that both Aβ40-Dutch and Aβ40-Iowa have strong propensities to form antiparallel β-hairpins in the first step of the fibrillization process. However, there is a marked difference in the ability of these peptides to form elongated antiparallel structures. Importantly, we find marked differences in the stability of the protofibril or fibril states formed by the four Aβ peptides. We discuss these differences with respect to the mechanisms of Aβ fibril formation in CAA.

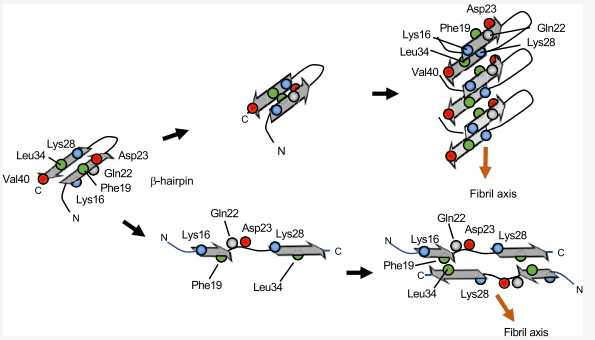

The amyloid-β (Aβ) peptides associated with Alzheimer's disease (AD) are generated by proteolytic cleavage of the transmembrane region of the amyloid precursor protein.[1] The peptides vary in length from ∼38 to 50 amino acids; however, nearly 90% are Aβ40 (40 residues in length), while 5−10% are Aβ42 (42 residues in length).[2] Senile plaques with a typical cored morphology in AD patients appear to be composed primarily of the longer Aβ42 peptide.[3,4] Early onset AD is correlated with an increase in the Aβ42/Aβ40 ratio that can arise due to widely dispersed mutations in presenilin or mutations near the Aβ coding region within the amyloid precursor protein.[5]

The Aβ40 peptide, however, is strongly associated with a second disease, cerebral amyloid angiopathy (CAA).[6] CAA is characterized by amyloid deposition in and around cerebral blood vessels.[7−10] The progressive accumulation of vascular amyloid leads to loss of blood vessel wall integrity and in severe cases intracranial hemorrhage. Parenchymal and vascular deposits are often observed together in aging individuals.[11,12] However, CAA can occur in the absence of AD.[13]

CAA can be differentiated into two distinct subtypes on the basis of the type of blood vessels affected.[14] Type 1, or capillary CAA, is predominantly characterized by amyloid deposition in cortical capillaries but may also be associated with deposits in other blood vessels. Conversely, CAA type 2 is most prominent in large cerebral vessels and has a lower propensity to form in or near cortical capillaries. Capillary deposits present in CAA type 1 appear to have enhanced levels of Aβ42 relative to those of Aβ40.[15−18] This type of CAA generally occurs in conjunction with AD pathology[15] and often leads to a robust perivascular neuroinflammatory response that is largely absent in CAA type 2.[19−21] In contrast, the large vascular deposits in CAA type 2 are enriched in Aβ40.[15−18] Typically, CAA type 2

Received: December 6, 2021
Revised: March 22, 2022
Published: June 6, 2022

cases lack the parenchymal amyloid plaques and neurofibrillary tau pathology that are key features of AD.[22−26]

The two types of CAA are best distinguished by the pathology resulting from different familial mutations in the amyloid precursor protein. The Aβ40-Iowa mutation (D23N)[27,28] is associated with CAA type 1, whereas the Aβ40-Dutch mutation (E22Q), the first familial CAA mutation to be described, is characteristic of CAA type 2[29,30] (Figure 1).

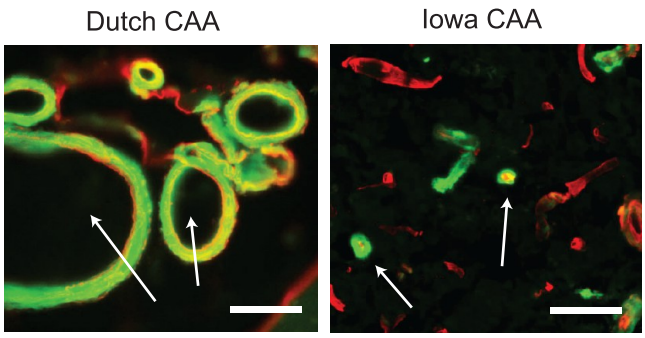

Figure 1. Comparison of cerebral vascular amyloid deposition in familial Dutch and Iowa CAA cases. Confocal images of cortical brain sections from Dutch (left) and Iowa (right) familial CAA patients. Cortical samples were immunolabeled for collagen type IV to identify cerebral blood vessels (red) and stained with thioflavin S to identify fibrillar amyloid deposits (green). The E22Q (Dutch) and D23N (Iowa) mutations both lead to enhanced vascular amyloid deposition and CAA. In the Dutch form of CAA, amyloid primarily accumulates in larger blood vessels (CAA type 2). The left panel shows a cross section through several large blood vessels (arrows) where there is substantial deposition in the walls of the blood vessels. In the Iowa form of CAA, amyloid deposition occurs in capillaries and microvessels (CAA type 1) in the brain. The right panel shows cross sections through several microvessels (arrows). Scale bars are 50 μm.

The factors or mechanisms involved in these specific deposition patterns are not known. Notably, the Aβ40-Dutch and Aβ40-Iowa mutations occur on neighboring residues in the middle of the Aβ sequence. Both substitute a negatively charged amino acid for a neutral amine, and both exhibit fibrillization kinetics that are faster than those of Aβ40-WT. The observation that two very similar mutations on neighboring residues lead to distinct deposition patterns provides a clue for establishing the potential factors distinguishing CAA type 1 and type 2.

Preferential binding of an antibody[31] and a dye[32] to vascular amyloid compared to parenchymal amyloid strongly suggests that there is a structural difference between CAA- and AD-specific Aβ fibrils. In solution, the Aβ40-WT and Aβ42-WT peptides have been found to form fibrils with a parallel, in-register orientation of the individual β-strands.[33−36] In contrast, the Aβ40-Iowa mutant has the capability to adopt distinct antiparallel fibrils under quiescent solution conditions.[37] These fibrils are unusual in having only a single layer of Aβ molecules along the fibril axis and exhibit a curvilinear morphology reminiscent of short worm-like protofibrils (see Figures S1 and S2). These structures are metastable and can be converted to parallel, in-register fibrils by sonication[38] or strong agitation.[39] Less is known about the structure of the Aβ40-Dutch mutant. However, similar to the D23N Iowa mutation, the E22K Italian mutation is correlated with enhanced CAA progression[40] and is associated with antiparallel fibrils under quiescent solution conditions.[41] More recently, antiparallel β-structure has been found to occur in vascular amyloid deposits in transgenic rodent brain[42,43] and human brain diagnosed with sporadic CAA.[44] Together, these results suggest the mechanisms that guide the assembly and stability of Aβ fibrils in solution may play a role in the formation of vascular amyloid in the brain.

Early aggregation kinetics, formation of Aβ with antiparallel β-structure, and protofibril or fibril stability are all potential factors that may influence vascular deposition of Aβ40-Dutch and Aβ40-Iowa. Comparisons are made with Aβ40-WT and Aβ42-WT for which the *in vitro* fibrillization mechanisms and fibril structures have been extensively characterized. In our studies, monomeric Aβ is first formed at 4 °C, and the fibrillization process is followed at ∼25 and 37 °C. The substitutions of a charged residue with a neutral amine in the E22Q and D23N mutants strongly suggest that both electrostatic and hydrophobic interactions influence the folding of Aβ and its association into vascular amyloid. The higher temperature favors hydrophobic interactions and parallel, in-register Aβ fibril structures, while the lower temperatures favor electrostatic interactions and potentially antiparallel protofibril or fibril assembly. The comparisons with Aβ40-WT and Aβ42-WT are also relevant because Aβ40-Dutch and Aβ40-WT are preferentially associated with CAA type 2 while Aβ40-Iowa and Aβ42-WT are preferentially associated with CAA type 1.[15,45] For example, patients with the Aβ40-Dutch mutation have lower levels of Aβ42 compared to those of patients with AD.[46] Together, the comparison of the solution properties of the Aβ peptides may provide insights into differences between CAA type 1 and CAA type 2.

Structural studies are undertaken here using Fourier transform infrared (FTIR) spectroscopy and both solution and solid-state nuclear magnetic resonance (NMR) spectroscopy. The FTIR measurements focus on the amide I vibration using a ^{13}C labeling scheme that is sensitive to antiparallel β-structure.[47] The solution NMR studies probe the stability of early intermediates in fibril formation, while solid-state NMR measurements make use of specific intermolecular dipolar couplings to measure the formation of parallel, in-register fibril structures.[47,48] Soluble oligomers and protofibrils having nonfibrillar and fibrillar antiparallel structures have been associated with cellular toxicity, and it has been a challenge to discriminate between these different forms.[48]

In comparison to the Aβ40-WT peptide, the Aβ40-Dutch and Aβ40-Iowa mutant peptides are both found to have strong propensities to form antiparallel β-hairpins in the first step of the fibrillization process. However, there is a marked difference in the ability of these peptides to form elongated antiparallel β-sheet structures. We find that Aβ40-Iowa has the strongest propensity to rapidly associate into antiparallel fibrils that are stable for weeks at 37 °C under low-ionic strength conditions and in the absence of strong agitation or sonication. These fibrils have a curvilinear morphology and only a single layer of the Aβ peptide (see Figure S1). In contrast, under the same experimental conditions, Aβ40-Dutch forms parallel, in-register fibrils. We discuss the similarities and differences between these peptides and how their solution properties provide insights into amyloid deposition and fibril structure in the human brain.

https://doi.org/10.1021/acs.biochem.1c00781
Biochemistry 2022, 61, 1181−1198

EXPERIMENTAL SECTION

Peptide Synthesis and Sample Preparation. Aβ peptides were synthesized using tBOC chemistry (ERI-Amyloid, Waterbury, CT) and purified by high-performance liquid chromatography. The mass of the purified peptide was measured using matrix-assisted laser desorption or electrospray ionization mass spectrometry and was consistent with the calculated mass of the peptide. On the basis of analytical reverse-phase high-performance liquid chromatography and mass spectrometry, the purity of the peptides was 95−99%.

The monomeric Aβ peptide was prepared by first dissolving purified peptides in hexafluoro-2-propanol (HFIP) and freeze-drying under a vacuum of 2−6 mTorr for 2 days. Lyophilized Aβ peptides were then dissolved in 100 μL of 50 mM NaOH per milligram of Aβ for 1 h, followed by dilution in 10 mM sodium phosphate buffer (pH 7.2−7.4) at 4 °C to a concentration of 100 μM. The pH and sodium phosphate buffer were selected to reflect physiological conditions. Two different concentrations of NaCl were used, 0 and 10 mM. The studies of Tycko and co-workers[37] showing that Aβ40-Iowa forms single-layer antiparallel fibrils were undertaken in the absence of NaCl, which favors electrostatic interactions and is perhaps a better mimic of the vascular membrane environment where Aβ40-Iowa exhibits enhanced deposition. One of the aims of this study was to investigate whether the Aβ40-Dutch peptide, which has a very similar mutation, has a similar propensity to form this unusual conformation. The addition of 10 mM NaCl serves to dampen electrostatic interactions and test whether these interactions dominate the structural transitions in the formation of Aβ40-Dutch and Aβ40-Iowa fibrils.

The solution was then filtered with 0.2 μm filters before use. In all cases, the samples were incubated with relatively slow (100 rpm) orbital shaking, except for the HSQC experiments and associated TEM measurements, which were carried out under quiescent conditions. Strong shaking or agitation is nonphysiological, while gentle shaking may better resemble the hydrodynamic flow created by the blood flow in the brain.[49] Strong shaking (≥200 rpm) can have a dramatic influence on the morphology of fibrils formed. For example, a recent cryo-electron microscopy (cryo-EM) study of tau fibrils in AD found that the structure of the brain-derived tau fibril could be reproduced *in vitro* only with slow shaking.[50] For both Aβ40-Dutch and Aβ40-Iowa, we have shown that strong shaking leads to formation of parallel, in-register fibrils. In a similar fashion, sonication is avoided due to local heating of the sample, which leads to rapid nucleation and elongation of the Aβ peptides. We have shown for Aβ40-WT, which takes days to form fibrils under slow shaking conditions at 25 °C, that sonication can drive fibril formation in a few hours.[44]

FTIR Spectroscopy. FTIR measurements were taken with a Bruker Vertex 70v spectrometer with a room-temperature detector and attenuated total reflectance (ATR) accessory. Samples were layered on a 2 mm germanium ATR plate (Pike Technologies) by drying 50 μL of the peptide sample on the plate surface with a stream of air. The spectral resolution was 4 cm^{-1}. The final spectra were normalized to the intensity of the amide II absorbance band, which is proportional to the peptide content.

Size Exclusion Chromatography. First, 200 μL of the prepared 100 μM Aβ samples was injected into an AKTA Pure 25L FPLC device with a Superdex 200 Increase 10/300 GL column (GE Healthcare) having a molecular weight (MW) range of 3−600 kDa. A flow rate of 0.3 mL/min was used, and the ultraviolet absorbance was recorded at 280 nm. The molecular mass for this column was calibrated by using the following proteins and/or molecules under the same separation conditions: aldolase (MW = 158 kDa), conalbumin (MW = 75 kDa), ovalbumin (MW = 44 kDa), carbonic anhydrase (MW = 29 kDa), RNase A (MW = 13.7 kDa), and aprotinin (MW = 6.5 kDa). The samples for SEC analysis were incubated at either room temperature or 37 °C with 100 rpm shaking and then injected onto the column kept at room temperature.

Transmission Electron Microscopy. Samples were diluted, deposited onto carbon-coated copper mesh grids, and negatively stained with 2% (w/v) uranyl formate. The excess stain was wicked away, and the sample grids were allowed to air-dry. The samples were viewed with a JEOL JEM-2100 instrument with a LaB6 filament running at 80 kV, and digital images were taken with an Advanced Microscopy Technique camera.

Atomic Force Microscopy. AFM images were obtained using a MultiMode microscope (Digital Instruments, Santa Barbara, CA) with a custom-built controller (LifeAFM, Port Jefferson, NY) that allows one low-force contact (30−50 pN) of the AFM tip to the sample surface per pixel. The single-touch approach is rapid and allows one to image a 1 μm × 1 μm field in ∼4 min. The AFM operation is embedded in a computer program that provides subangstrom linear control of the cantilever base and tip position, including programmed contact and programmed separation of the tip by a magnetic force ramp. Supersharp silicon probes with a tip width of typically 3−5 nm (at a height of 2 nm) were modified for magnetic retraction by attachment of samarium cobalt particles. Samples for AFM were diluted to a concentration of 0.5 μM, deposited onto freshly cleaved ruby mica (S & J Trading, Glen Oaks, NY), and imaged under hydrated conditions.

Solid-State NMR Spectroscopy. Solid-state NMR experiments were performed at a ^{13}C frequency of 125 or 150 MHz on a Bruker AVANCE spectrometer using a 4 mm MAS probe. The MAS spinning rate was set to 10−12 kHz (±5 Hz) depending on the labeling scheme of each given sample such that possible cross-peaks do not overlap with spinning sidebands and/or folded/aliased resonances in the two-dimensional (2D) experiments. Internuclear $^{13}C\cdots^{13}C$ distance constraints were assessed from the presence and intensity of cross-peaks obtained in 2D dipolar-assisted rotational resonance (DARR) NMR experiments.[51] In these experiments, the initial ^{13}C magnetization is generated by a ramped amplitude cross-polarization sequence with a contact time of 2 ms. The evolution under proton decoupling is followed by a single nonselective 90° pulse to store the chemical shift-encoded ^{13}C magnetization along the *Z* axis. Mixing occurs along this axis under a proton decoupling field strength (measured in hertz) equal to the spinning speed of the sample for a duration of 600 ms. This low-field decoupling results in the broadening of the ^{13}C resonances, allowing energy exchange through a rotational resonance effect. A second nonselective 90° pulse generates the observable magnetization, recorded during t2. Two-pulse phase-modulated decoupling was used during the evolution and acquisition periods with a radiofrequency field strength of ∼80 kHz.

For the solid-state NMR experiments, the Aβ peptides were labeled with unique amino acids at specific positions in the

https://doi.org/10.1021/acs.biochem.1c00781
Biochemistry 2022, 61, 1181−1198

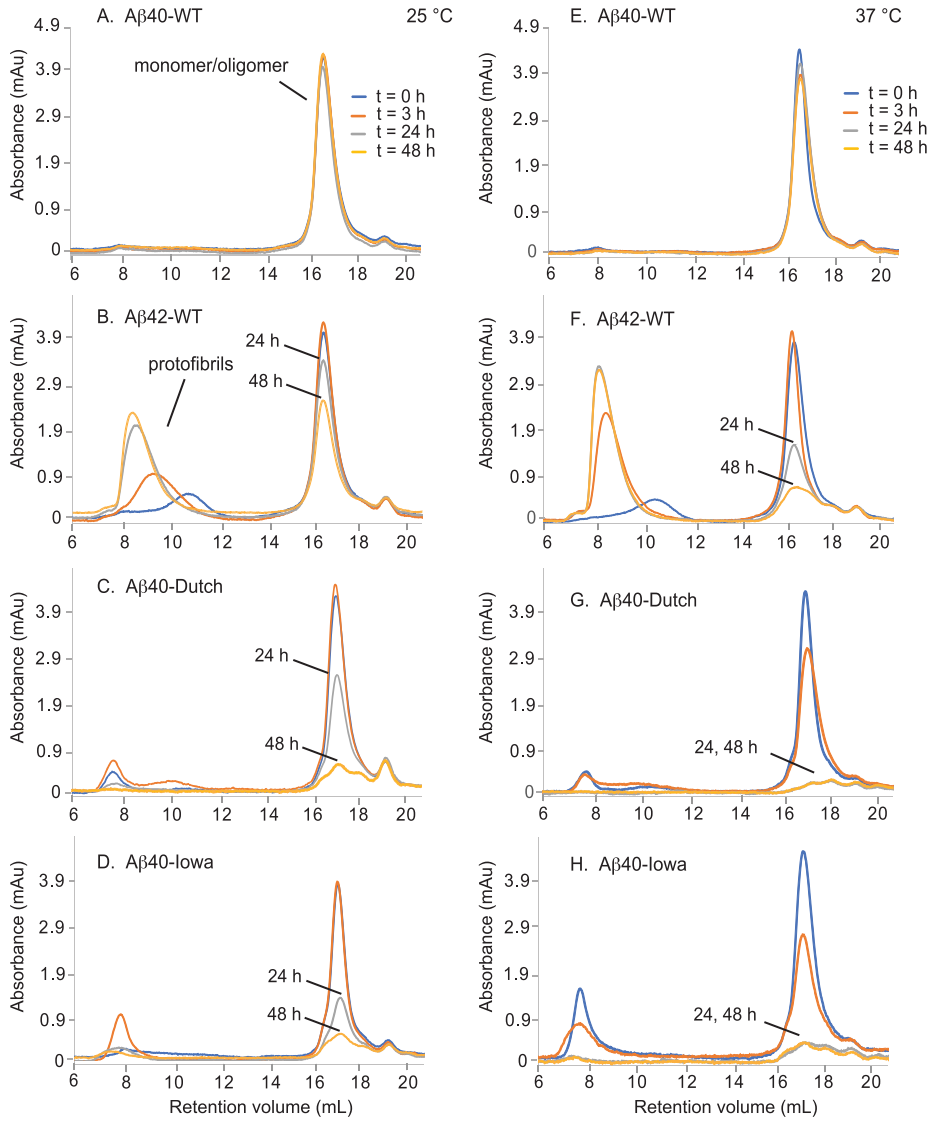

Figure 2. Size exclusion chromatography of Aβ40-WT, Aβ42-WT, Aβ40-Dutch, and Aβ40-Iowa. Size exclusion chromatograms are shown for the Aβ peptides incubated at (A−D) ∼25 and (E−H) 37 °C as a function of incubation time. Generally, these peptides elute in two major fractions. The first fraction at ∼8 mL contains protofibrils, while the second fraction at ∼17 mL contains monomers and oligomers. Stable fibrils are excluded from entering the SEC column. The samples were prepared at 4−6 °C at time zero and immediately injected into the SEC column, which was at room temperature.

sequence chosen for their non-overlapping chemical shifts and their potential as probes of specific structural features. The assignments can be made readily on the basis of the known chemical shifts, either directly in the one-dimensional spectrum or by using the position of the resulting $^{13}C-^{13}C$ cross-peaks in the 2D experiments.

All ^{13}C solid-state MAS NMR spectra were externally referenced to the ^{13}C resonance of neat tetramethylsilane at 0 ppm at room temperature. Using tetramethylsilane as the external reference, we calibrated the carbonyl resonance of solid glycine at 176.46 ppm. The chemical shift difference between ^{13}C of DSS in D_2O relative to neat tetramethylsilane is 2.01 ppm.

Solution-State NMR Spectroscopy. Solution-state NMR experiments were performed at a ^1H frequency of 850 MHz on a Bruker AVANCE spectrometer. The 100 μM samples of Aβ40-WT, Aβ42-WT, Aβ40-Iowa, and Aβ40-Dutch containing ^{15}N labels at Gly9, Gly29, Gly33, and Gly37 were prepared as described above. Then, 10% (v/v) deuterated water was added to all samples to lock the B_o field. An initial spectrum was taken at 4 °C and was used as a reference for 100% monomer. The temperature was subsequently increased to either 25 or 37 °C, and another spectrum was collected. The samples were then incubated at the higher temperature under quiescent conditions. For further readings at 3, 24, and 48 h, the sample temperature was decreased to 4 °C and a spectrum was acquired. Immediately afterward, the temperature was increased and another spectrum acquired. Each ^{15}N HSQC spectrum contains eight scans. Peak volumes were extracted at each time point and normalized to the time zero peak intensities. Normalized values were averaged across all four ^{15}N labels; error bars represent the standard deviation.

Histology. Fresh frozen autopsy cortical tissue samples from familial Dutch and Iowa CAA cases were provided by S. van Duinen (Department of Pathology, Leiden University Medical Center, Leiden, The Netherlands) and M. Frosch [Director, Massachusetts Alzheimer's Disease Research Center

https://doi.org/10.1021/acs.biochem.1c00781
Biochemistry 2022, 61, 1181−1198

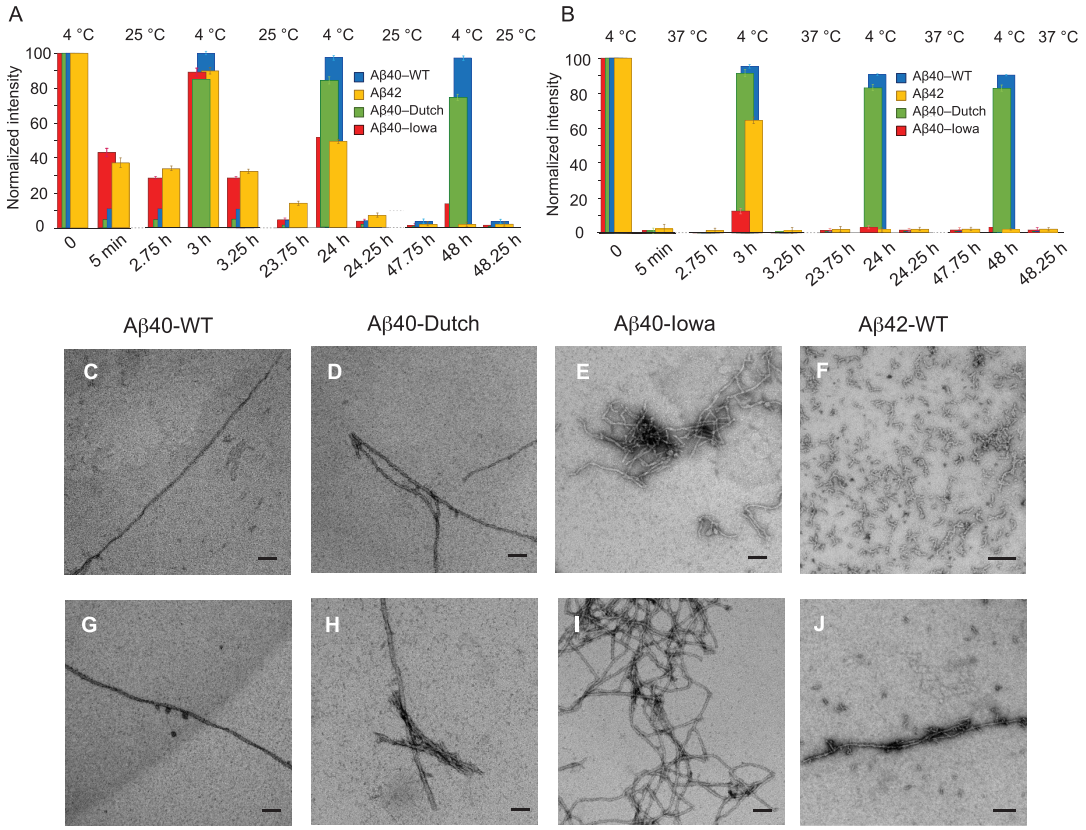

Figure 3. Solution NMR analysis of fibril formation of Aβ40-WT, Aβ42-WT, Aβ40-Dutch, and Aβ40-Iowa. Influence of temperature cycling on the $^{1}H-^{15}N$ HSQC resonances of the four Aβ peptides. The temperature was cycled between 4 °C and either (A) 25 or (B) 37 °C. The intensity of the $^{1}H-^{15}N$ HSQC NMR resonances was measured at 4 °C immediately after preparation and filtering of the Aβ samples at this temperature. Peak volumes were extracted at each time point and normalized to the time zero peak intensities. Normalized values were averaged across all four ^{15}N labels; error bars represent the standard deviation. Aggregation of monomeric Aβ into oligomers, protofibrils, and fibrils as the samples are incubated at higher temperature results in the loss of NMR intensity. Incubation for the HSQC experiments was performed under quiescent conditions. (C–J) TEM images of fibril formation of Aβ40-WT, Aβ42-WT, Aβ40-Dutch, and Aβ40-Iowa. TEM micrographs of Aβ40-WT, Aβ42-WT, Aβ40-Dutch, and Aβ40-Iowa are shown after incubation for 24 h at (C–F) 25 and (G–J) 37 °C. The TEM samples were prepared from the samples used in the NMR analysis. Scale bars are 50 nm.

(P50 AG005134), Charlestown, MA], respectively. Each brain sample was confirmed to possess the Dutch or Iowa familial CAA mutation in the amyloid precursor protein by genotyping and by neuropathological analysis. Tissue samples were embedded in OCT compound (Sakura Finetek Inc., Torrance, CA). Sections were cut at a 12 μm thickness from frozen brains using a Leica CM1900 cryostat (Leica Microsystems Inc., Bannockburn, IL) and then mounted on Colorfrost/Plus slides (Fisher Scientific, Houston, TX). The primary rabbit polyclonal antibody to collagen type IV was used to visualize cerebral microvessels (1:100; ThermoFisher, Rockford, IL). The primary antibody was detected with the Alexa Fluor 594-conjugated donkey anti-rabbit secondary antibody (1:1000). Staining for fibrillar amyloid was performed using thioflavin S. Images of the brain sections were collected using a Keyence BZ-X710 microscope (Keyence Corp., Itasca, IL).

RESULTS

Aβ40-Iowa and Aβ40-Dutch Rapidly Form Fibrils via Protofibril Intermediates. One of the distinguishing features of familial mutants of the Aβ peptides is their rapid fibrillization rates compared to those of the wild-type sequences.[52,53] In addition to the specific amino acid sequence, the rate and mechanism of Aβ fibril formation are known to be dependent on several additional factors, including temperature and concentration. The experiments described below were undertaken at a single concentration (100 μM) and at ~25 or 37 °C. These temperatures are often used for *in vitro* studies of Aβ fibrillization. For example, nuclear conformational conversion via oligomeric intermediates is favored for Aβ42-WT at 37 °C, while fibril formation via nucleated polymerization can occur at lower temperatures and at higher monomeric concentrations.[48] A third variable that has a strong influence on the rate and mechanism of fibril formation is agitation of the sample.[34] Strong agitation favors the formation of laterally associated fibrils, while quiescent conditions or slow agitation leads to twisted fibrils composed of two or more protofilaments.[34] Here, we rotated the samples at 100 rpm during incubation, a rate that is not strong enough to form laterally associated fibrils.

There are several methods for following the time course of Aβ fibrillization. These include thioflavin T fluorescence spectroscopy, light scattering, and size exclusion chromatography (SEC). SEC has the advantage of being able to distinguish monomers and small oligomers from protofibrils and fibrils at different time points during the fibrillization time course. On the basis of SEC measurements and cross-linking studies, Bitan and co-workers found that Aβ40-WT and Aβ42-WT fibrils form via different oligomeric intermediates.[54] High-

https://doi.org/10.1021/acs.biochem.1c00781
Biochemistry 2022, 61, 1181–1198

molecular weight oligomers of Aβ42-WT (pentamers to dodecamers) rapidly aggregate to form protofibrils,[48] whereas the aggregation of Aβ40-WT at comparable concentrations and temperatures only slowly gives rise to fibrils via dimer, trimer, and tetramer intermediates.[54]

The comparison of Aβ40-WT and Aβ42-WT shown in Figure 2 mirrors the conclusions from previous SEC studies.[48,54] In the SEC profile of Aβ42-WT, monomers and oligomers (at least up to dodecamers) elute in the broad band at 17 mL at both 25 and 37 °C[48] (Figure 2B,F). This band is attributed predominantly to oligomers due to a rapid conversion of monomers to oligomers[48] (see Figure 3). The bands stretching from 8 to 11 mL are attributed to protofibrils (Figure 2B). Protofibrils are formed by the lateral association of oligomers and can have a range of sizes from ∼200 to >600 kDa, corresponding to the molecular weight cutoff of the SEC column used (Figure S1). As the protofibrils undergo the transition into β-sheet fibrils, they are excluded from the SEC column.[55]

In contrast to Aβ42-WT, Aβ40-WT exhibits markedly different SEC elution profiles (Figure 2A,E) over the time and temperature ranges that were measured. Higher concentrations and higher temperatures lead to the formation of oligomers and protofibrils.[48] At both 25 and 37 °C, the peptide results in a single elution band at ∼17 mL, although replicate experiments can yield a small protofibril peak.

The SEC measurements of Aβ40-WT and Aβ42-WT provide a baseline for comparison of Aβ40-Dutch and Aβ40-Iowa (Figure 2C,D). For these mutant Aβ40 peptides, the rate of transition from monomers and small oligomers to fibrils is notably impacted by temperature and increases at 37 °C compared to 25 °C. Under both conditions and for both mutants, the monomer/oligomer peak is largely absent at 48 h, consistent with the rapid rate of fibril formation. Both familial Aβ mutants exhibit protofibril intermediates (Figure S2). However, the concentration of protofibrils is small compared to that of Aβ42-WT where the protofibril intermediates are clearly in the pathway between oligomers and fibrils. SEC measurements on the E22G Aβ40-Arctic peptide (data not shown) also exhibit protofibril peaks resembling the Aβ42-WT traces similar to what has been observed previously.[56,57]

Stability of Protofibrils and Fibrils Formed by Different Aβ Peptides. Monomeric Aβ is favored at low temperatures.[58] At temperatures between 4 and 10 °C and at a concentration of 60 μM, monomeric Aβ40-WT remains stable for weeks.[58] For Aβ42-WT, monomeric Aβ more aggressively aggregates to form oligomers and protofibrils as the temperature is increased (see, for example, Figure 2). To explore potential differences in the intrinsic solution properties of Aβ40-WT, Aβ42-WT, Aβ40-Iowa, and Aβ40-Dutch, we followed the influence of temperature on monomeric Aβ using temperature-cycling solution NMR spectroscopy.[59] In these experiments, monomers of the Aβ peptides exhibit sharp $^{1}H-^{15}N$ resonances in 2D heteronuclear single-quantum correlation (HSQC) NMR spectra.[60] For both Aβ40-WT and Aβ42-WT, as the sample temperature is increased, the resonances broaden and intensity is lost.[48] The broadening may result from a shift of the monomers to higher-MW species or may be due to conformational changes in the protein.

For Aβ42-WT, we have previously shown by cycling the temperature from 25 or 37 °C back to 4 °C that the protofibril peaks in the SEC chromatograms will shift back to monomers or small oligomers.[48] (In these studies, NMR diffusion measurements showed that the low-temperature form of Aβ42-WT was closer to a monomer or dimer than a hexamer.) We interpret the ability to shift back to the monomer−dimer state as a function of oligomer or protofibril stability. As intermolecular β-sheet structure forms in the transition of Aβ42-WT protofibrils to fibrils, decreasing the temperature is less effective in disaggregating Aβ42-WT.[48] Note that in these experiments we typically only cycle the temperature back to 4 °C for ∼30 min. As a result, the extent of disaggregation is actually a function of the rate of disaggregation (i.e., kinetics), which is slowed as cross β-sheet fibrils form.[48]

For Aβ40, the loss of intensity due to an increase in temperature has been associated with β-hairpin formation with a turn between Asp23 and Ala30.[59] This interpretation is consistent with the SEC profiles of Aβ40 shown in Figure 3, where only a single band comprised of monomers and small oligomers is observed. Cross-linking studies of Aβ40 reveal that the predominant oligomers are dimers, trimers, and tetramers in rapid equilibrium.[54]

For our studies here, we focused on the glycine resonances that are easily assigned in the HSQC spectrum and have been shown to be the most sensitive to temperature changes.[59] In the monomeric Aβ peptides prepared at 4 °C, these resonances are intense. Increasing the temperature to 25 °C leads to a rapid loss of intensity in all four peptides (Figure 3A). The largest intensity changes are for Aβ40-WT and Aβ40-Dutch.

Recooling the samples after incubation for 3 h recovers most of the intensity for all peptides. The HSQC intensity continues to decrease after incubation for 24 and 48 h at 25 °C. Cooling after incubation for 24 h to 4 °C results in almost complete return of the intensity for Aβ40-WT and Aβ40-Dutch, and ∼50% intensity for Aβ40-Iowa and Aβ42-WT. After 48 h, the intensity for Aβ42-WT and Aβ40-Iowa does not return upon recooling. Unlike Aβ40-WT, the Aβ40-Dutch and Aβ40-Iowa peptides aggregate rapidly over the 48 h time course of this experiment and the loss of intensity likely reflects this aggregation process. Below we address the ability of Aβ40-WT, Aβ40-Dutch, and Aβ40-Iowa to form β-hairpin structures as monomers or small oligomers under the temperature and concentration conditions explored here.

Parallel temperature-cycling measurements between 4 and 37 °C show a similar but more striking pattern (Figure 3B). Immediately after the samples had been heated to 37 °C, the intensity is completely lost for all four peptides. At 24 h, there is a distinct difference between the Aβ peptides associated with CAA type 1 (Aβ40-Iowa and Aβ42-WT) and CAA type 2 (Aβ40-Dutch and Aβ40-WT). The spectra of the Aβ40-Dutch and Aβ40-WT peptides regain intensity upon recooling to 4 °C after 24 h, while no intensity is observed for Aβ40-Iowa or Aβ42-WT.

TEM provides a qualitative measure of the state of the Aβ peptides as a function of incubation time and temperature. After incubation for 24 h at 25 °C, long fibrils are observed for Aβ40-Dutch and Aβ40-Iowa (Figure 3D,E). For Aβ42-WT, protofibrils, characterized by nonfilamentous appearance, are the dominant visible form at 24 h and remain for more than 2 weeks at 25 °C (Figure 3F). For Aβ40-WT, a few fibrils are observed at 25 °C, but they are very sparse on the TEM grids (Figure 3C). The suggestion from the SEC data is that when the Aβ40-WT oligomers undergo a conformational transition, they can rapidly polymerize via monomer addition. The Aβ40-Dutch (Figure 3D) and Aβ40-Iowa (Figure 3E) species readily

https://doi.org/10.1021/acs.biochem.1c00781
Biochemistry 2022, 61, 1181−1198

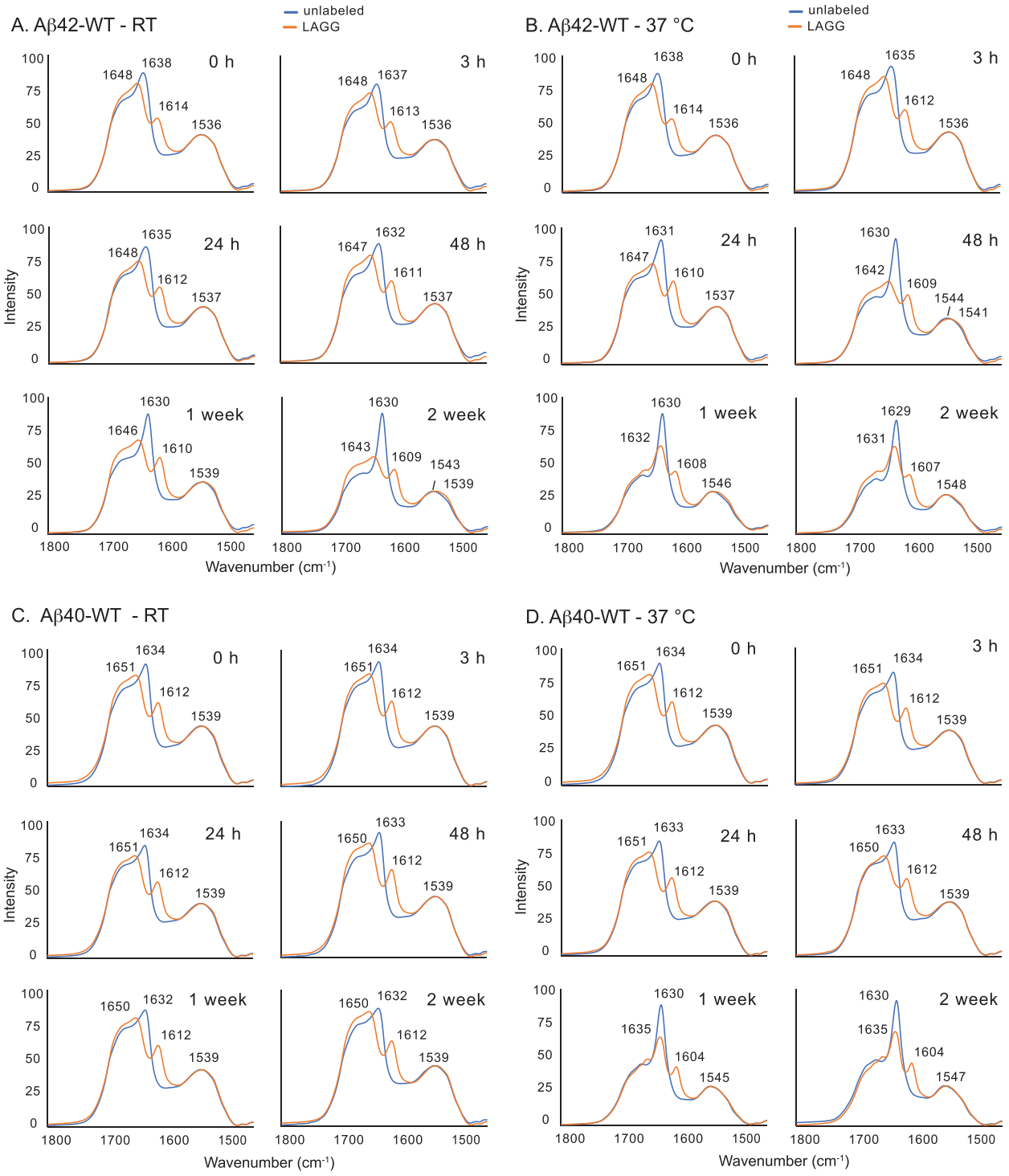

Figure 4. FTIR spectra of Aβ42-WT and Aβ40-WT. FTIR spectra of the (A and B) Aβ42-WT and (C and D) Aβ40-WT peptides were recorded as a function of incubation time at ~25 and 37 °C. For each incubation time point, samples were run in parallel with and without ^{13}C labeling (black trace) and with ^{13}C-LAGG labeling (red trace) having backbone ^{13}C═O labels at Leu17, Ala21, Gly33, and Gly37. The final spectra were normalized to the intensity of the amide II absorbance band.

form fibrils more reliably than Aβ40-WT, although the Iowa mutant adopts a curvilinear appearance.

After incubation for 24 h at 37 °C, fibrils can be observed for all four peptides by TEM (Figure 3G–J). As at 25 °C, the Aβ40-WT fibrils are very sparse on the TEM grids (Figure 3G) while both Aβ40-Dutch and Aβ40-Iowa are much more abundant. The Aβ40-Iowa fibrils retain their curvilinear structure (Figure 3I). Aβ42-WT has undergone the transition from protofibrils to fibrils at the higher temperature (Figure 3J).

FTIR Spectroscopy as a Probe of the Antiparallel Structure in Aβ Peptides. The hallmark of Aβ fibril formation is the conversion to cross β-sheet structure. FTIR spectroscopy complements the methods described above by providing a time course for β-sheet formation by following the frequency shifts of the amide I and II vibrations (Figure S3).

https://doi.org/10.1021/acs.biochem.1c00781
Biochemistry 2022, 61, 1181−1198

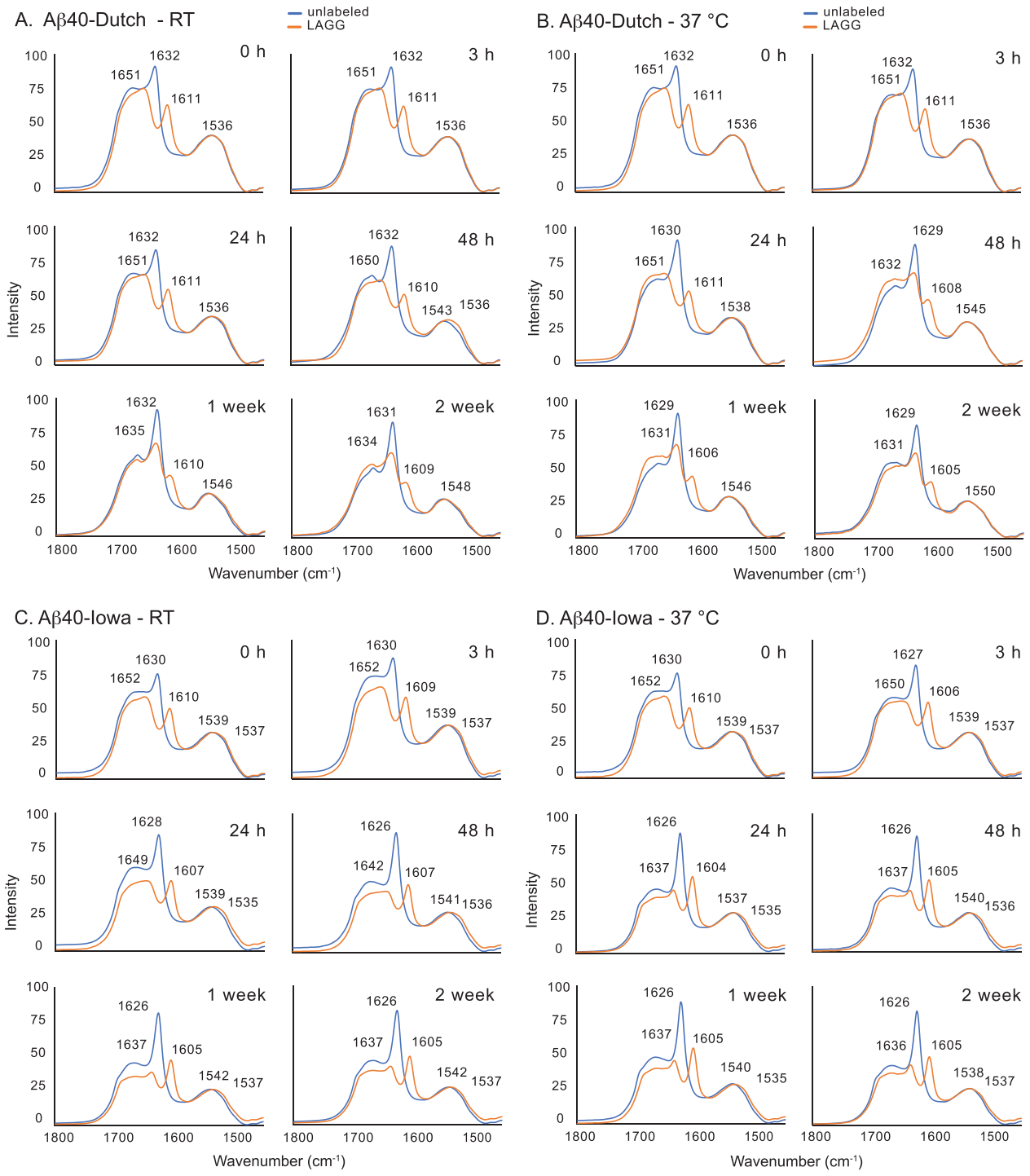

Figure 5. FTIR spectra of Aβ40-Dutch and Aβ40-Iowa. FTIR spectra were obtained of the (A and B) Aβ40-Dutch and (C and D) Aβ40-Iowa peptides as a function of incubation time at 25 and 37 °C. For each incubation time point, samples were run in parallel with and without ^{13}C labeling (blue trace) and with ^{13}C-LAGG labeling (red trace) having backbone ^{13}C═O labels at Leu17, Ala21, Gly33, and Gly37. The final spectra were normalized to the intensity of the amide II absorbance band.

When combined with ^{13}C labeling of the backbone carbonyl, the amide I vibration provides an excellent probe of distinguishing changes in the secondary structure of amyloid peptides as a function of time.[61] One of the striking differences between Aβ40-Iowa and the other peptides is its ability to form antiparallel β-sheet fibril structure.[37] In studies of Aβ peptides, antiparallel structure is most often associated with oligomers and protofibrils.[62,63] For Aβ42-WT, we have shown that the peptide rapidly adopts an antiparallel β-hairpin prior to forming cross-β sheet fibrils.[48] More recently, antiparallel β-hairpin structure has been proposed for Aβ40-Dutch and Aβ40-Iowa.[39] The SEC and HSQC NMR experiments described above provide time courses at 25 and 37 °C for the aggregation of Aβ but do not address whether cross-β sheet fibrils have formed. We have previously introduced an FTIR method for monitoring the conversion of monomers to fibrils that provides a way to distinguish antiparallel and parallel β-structure[47] (see also Figure S4).

https://doi.org/10.1021/acs.biochem.1c00781
Biochemistry 2022, 61, 1181−1198

The amide I vibrational modes at ∼1626−1635 cm^{-1} in the FTIR spectrum are associated with β-sheet secondary structure.[42] Specific ^{13}C labeling of the backbone C═O group along the Aβ sequence results in an isotope-induced shift of the β-sheet normal mode to lower frequency and can be used to assess the presence of parallel and antiparallel β-sheet. Our previous study describes the details of this method.[47] Briefly, four ^{13}C labels are included within the two hydrophobic patches of the peptide, which provides a better probe for antiparallel structures.[39,48] Two of the 1-^{13}C labels are in the first hydrophobic stretch of amino acids, namely, at 1-^{13}C-Leu17 and 1-^{13}C-Ala21, while the second two 1-^{13}C labels are at 1-^{13}C-Gly33 and 1-^{13}C-Gly37. We refer to this peptide as ^{13}C-LAGG-labeled Aβ reflecting the labels being at Leu17, Ala21, Gly33, and Gly37. In antiparallel structures, the lower- and higher-frequency bands resulting from the isotope-induced split of the 1626 cm^{-1} band (diagnostic of β-sheet secondary structure) share intensity.[64,65] The greater the intensity of the lower-frequency ∼1607 cm^{-1} band, the larger the contribution of antiparallel β-structure.

Time Course for the Formation of Antiparallel Structure in Aβ Peptides. The FTIR ^{13}C labeling strategy described above provides an approach for following the evolution of antiparallel structure during fibril formation. In this section, we compare the structural transitions of all four Aβ peptides being studied to assess their relative propensity for forming antiparallel fibrils at ∼25 and 37 °C. The peptides were all incubated at 100 μM using Aβ peptides lacking ^{13}C═O labels as well as peptides with the ^{13}C-LAGG labeling scheme. The use of unlabeled Aβ provides a measure of the conversion of Aβ monomers to mature fibrils. The ∼1630 cm^{-1} band in the amide I region gains intensity and narrows as mature fibrils form. The use of the LAGG ^{13}C labeling scheme provides a measure of the contribution of antiparallel structure as described above.

The transition from monomers to fibrils can be followed via the 1630−1638 cm^{-1} band as a function of time in the unlabeled FTIR spectra (blue curves) at 37 °C for Aβ42-WT (see Figure 4B). This band is broad with a frequency of 1638 cm^{-1} at time zero and narrows to a sharp resonance at 1630 cm^{-1} after incubation for 2 weeks. The narrowing and shift to a lower frequency are associated with the formation of mature fibrils. The shift of the amide I band in the formation of fibrils is accompanied by a shift of the amide II band from ∼1535−1540 to ∼1545−1550 cm^{-1}. We have previously correlated these transitions with circular dichroism measurements, which provide a complementary approach for measuring changes in protein secondary structure.[48]

The FTIR spectrum of Aβ42-WT at time zero reflects a mixture of random coil and β-sheet secondary structure, where random coil results in a broad featureless amide I band while β-sheet (or β-hairpin) results in the narrower 1630−1638 cm^{-1} band. The use of the ^{13}C-LAGG-labeled peptide (red traces, Figure 4) allows us to characterize this initial structure as β-hairpin. FTIR spectra were recorded after filtering monomeric Aβ42 at 4 °C and layering on the ATR plate for IR measurements. As a result, the peptide can aggregate to form oligomeric species prior to the FTIR measurements (see HSQC analysis). In the FTIR spectrum at time zero, the ^{13}C labeling results in a splitting of the 1638 cm^{-1} resonance into a resonance at 1614 and 1648 cm^{-1}. The relative intensity of these two bands reflects the contribution of antiparallel structure (see Figure S4).

At 25 °C (Figure 4A), the amide I band in the FTIR spectra of unlabeled Aβ42-WT takes 2 weeks to narrow and increase in intensity, which is characteristic of mature fibrils. In contrast to the unlabeled FTIR spectra of Aβ42-WT, the spectra of ^{13}C-LAGG-labeled Aβ42-WT (red traces) suggest that there is still considerable antiparallel β-structure after incubation for 1−2 weeks. TEM images obtained after incubation for 2 weeks show both protofibrils and fibrils (Figure S5), suggesting that the antiparallel structure arises from the protofibrils.

At 37 °C (Figure 4B), the amide I band of unlabeled Aβ42-WT begins to narrow and increase in intensity after 48 h. The SEC traces presented previously indicate that there is still a substantial protofibril population after 48 h. A shift of the amide I band to 1629 cm^{-1} and the amide II band to 1548 cm^{-1} after incubation for 2 weeks indicates the formation of mature fibrils. In the ^{13}C-LAGG-labeled spectra, the intensity of the 1614 cm^{-1} band increases and then decreases as previously observed,[48] indicating the transient formation of β-hairpin structure.

The FTIR spectra of Aβ40-WT (Figure 4C,D) obtained as a function of incubation time exhibit several differences compared to those of Aβ42-WT. First, at 25 °C there is no clear transition to mature fibrils over 2 weeks. The broad 1634 cm^{-1} band shifts only slightly to 1632 cm^{-1} and remains broad. The amide II vibration remains at 1539 cm^{-1}. These observations are consistent with the thioflavin T and SEC results, and the known slower aggregation kinetics of Aβ40-WT relative to those of Aβ42-WT. Second, the ∼1612 cm^{-1} band in the time zero ^{13}C-LAGG-labeled spectra is more intense for Aβ40-WT than for Aβ42-WT, suggesting a higher percentage of β-hairpin structure.

Aβ40-Dutch and Aβ40-Iowa exhibit distinctive differences compared to Aβ40-WT and Aβ42-WT (Figure 5). First, there is a strong 1611 cm^{-1} resonance in the time zero spectra of the ^{13}C-LAGG-labeled peptides at both 25 and 37 °C, reflecting a substantial population of β-hairpin. Second, fibrils form rapidly for Aβ40-Iowa as reflected in the formation of a sharp band at 1626−1628 cm^{-1} in the unlabeled spectra (blue traces) at both temperatures. In addition, the intensity of the 1605−1610 cm^{-1} band remains intense, indicating that the peptide remains antiparallel. Solid-state NMR and TEM measurements of Aβ40-Dutch and Aβ40-Iowa at the 2 week time point show that at this time point Aβ40-Dutch has converted to long, twisted fibrils with parallel, in-register β-strands while the Aβ40-Iowa peptide exhibits intermolecular contacts that are characteristic of the antiparallel species described by Qiang et al.[37] (Figure S6).

An overlay of the FTIR spectra of the four Aβ peptides at time zero highlights the antiparallel β-hairpin that forms in the monomeric or oligomeric Aβ peptides (Figure S7A). The 1611 cm^{-1} band (see the expansion in Figure S7A) is the most intense for the Aβ40-Iowa and Aβ40-Dutch mutants and is markedly less intense for Aβ40-WT and Aβ42-WT. As the Aβ peptides are allowed to incubate at 25 and 37 °C, the β-sheet resonance begins to narrow and shift to a lower frequency. In panels B and C, the FTIR spectra at 3 h are shown for the four unlabeled Aβ peptides. These spectra highlight the rapid fibril formation of Aβ40-Dutch and Aβ40-Iowa compared to the two wild-type Aβ peptides and suggest that the ability to transiently form antiparallel β-hairpin structure (panel A) facilitates the conversion to cross-β sheet fibrils.

Comparison of the FTIR spectra of the four LAGG-labeled Aβ peptides after incubation for 2 weeks at 37 °C highlights

https://doi.org/10.1021/acs.biochem.1c00781
Biochemistry 2022, 61, 1181−1198

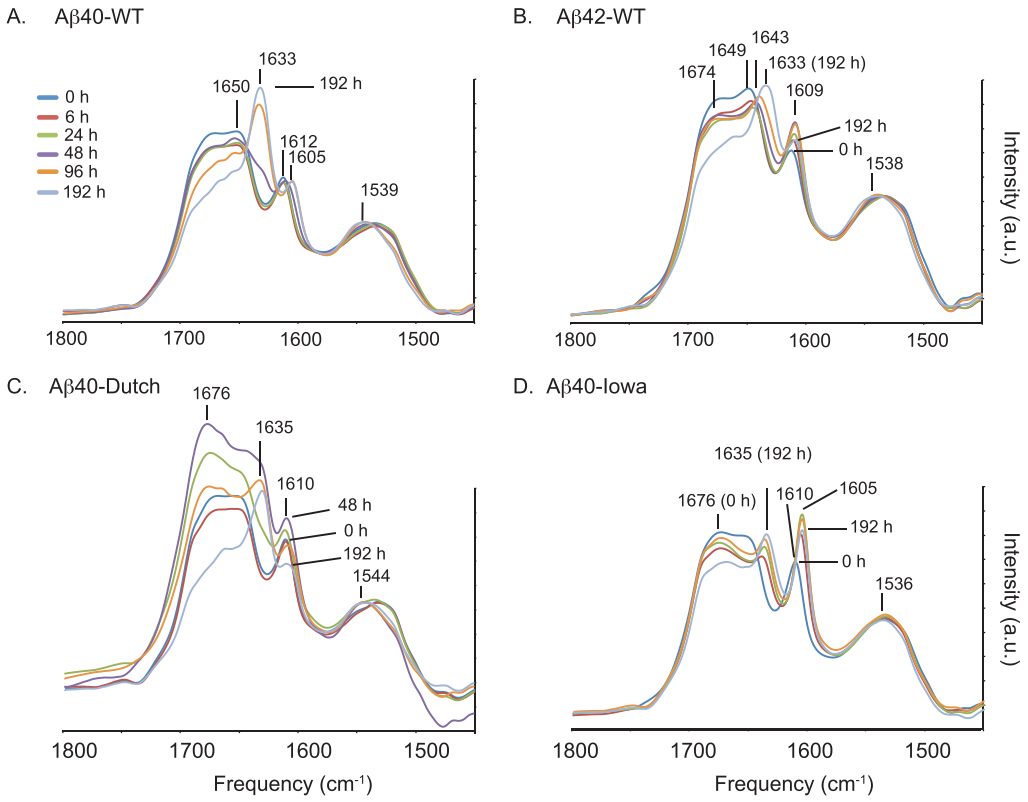

Figure 6. Influence of salt on the FTIR spectra of Aβ40-WT, Aβ40-Dutch, Aβ40-Iowa, and Aβ42-WT. FTIR spectra of the four peptides are shown with the addition of 10 mM NaCl. The striking feature with the addition of salt is the transient increase in the intensity in the spectra of the Aβ40-Dutch peptide during fibril formation at 1670−1680 cm^{-1}, which is interpreted as an increase in the level of random coil structure. An alternative explanation is that this band results from novel α-sheet structure described by Dagget and co-workers.[68] The temperature was maintained at 37 °C during incubation.

their relative propensities to form antiparallel structures (Figure S7D). In contrast to β-hairpin formation, only Aβ40-Iowa has a strong propensity for forming antiparallel fibrils as seen in the strong 1610 cm^{-1} band. However, as indicated above, these are the single-layer fibrils (Figure S2).

Influence of Salt on Aβ Fibril Formation. Aβ fibril formation is influenced by a wide range of factors. The temperature and sample agitation have a marked influence on fibrillization kinetics and fibril morphology. The buffer pH and ionic strength also influence fibril formation.[66,67] An increase in ionic strength results in an increase in the level of aggregation of Aβ as well as an increase in the rate of fibril formation.[66,67] The studies described here have been undertaken at a low ionic strength to disfavor the formation of nonfibrillar Aβ aggregates, to decrease the rate of fibril formation and to favor antiparallel structure as it forms. In this section, parallel FTIR time courses of the four Aβ peptides were undertaken using the ^{13}C-LAGG labeling scheme and with the addition of 10 mM NaCl to increase the ionic strength. These data highlight a difference between the Aβ40-Dutch peptide and the other three peptides.

The time for conversion of monomeric Aβ to mature fibrils, as reflected in the amide I and II vibrations, is roughly the same with the addition of 10 mM NaCl for the four Aβ peptides. In a similar fashion, the ∼1610 cm^{-1} band reveals substantial antiparallel β-hairpin structure in monomeric Aβ40-Dutch and Aβ40-Iowa (Figure 6C,D). However, a striking difference is the increase in a broad band at ∼1670−1680 cm^{-1} at 48 h in Aβ40-Dutch (Figure 6C). This change in the FTIR spectrum is reproducible and attributed to a transient increase in the level of random coil structure in the conversion from β-hairpin to fibrils (see Discussion). In contrast, increasing the ionic strength with 10 mM NaCl does not have a marked effect on the formation of antiparallel structure in Aβ40-Iowa.

NMR Spectroscopy as a Probe of Antiparallel β-Hairpin Formation. Phe19 is located in the central hydrophobic stretch of amino acids in the Aβ sequence, and Leu34 occurs in the C-terminal stretch of hydrophobic residues. Solid-state NMR studies of β-hairpin formation in Aβ42-WT have shown close packing of the side chains of Phe19 and Leu34[69] as a result of the central and C-terminal β-strands associating within Aβ monomers or small oligomers at early time points in the pathway to fibrils. In addition, mutational studies have argued that these residues form a critical folding contact in Aβ40-WT responsible for toxicity.[70] Close Phe19−Leu34 contacts in Aβ40-WT are consistent with close Glu22−Ile31 contacts observed in Aβ40-WT prior to the formation of mature fibrils.[71]

To probe whether the rapid formation of β-hairpin in the Aβ40-Dutch and Aβ40-Iowa peptides leads to similar packing of Phe19 and Leu34, solid-state ^{13}C MAS NMR experiments were undertaken after monomer formation at 4 °C. Parallel experiments were also undertaken with mature fibrils formed as a result of incubation for 2 weeks at 37 °C. Close Phe19−Leu34 interactions were measured with peptides containing ring ^{13}C-labeled Phe19 and uniformly ^{13}C-labeled Leu34 using dipolar-assisted rotational resonances (DARR). The DARR NMR approach restores ^{13}C···^{13}C dipolar couplings under

https://doi.org/10.1021/acs.biochem.1c00781
Biochemistry 2022, 61, 1181−1198

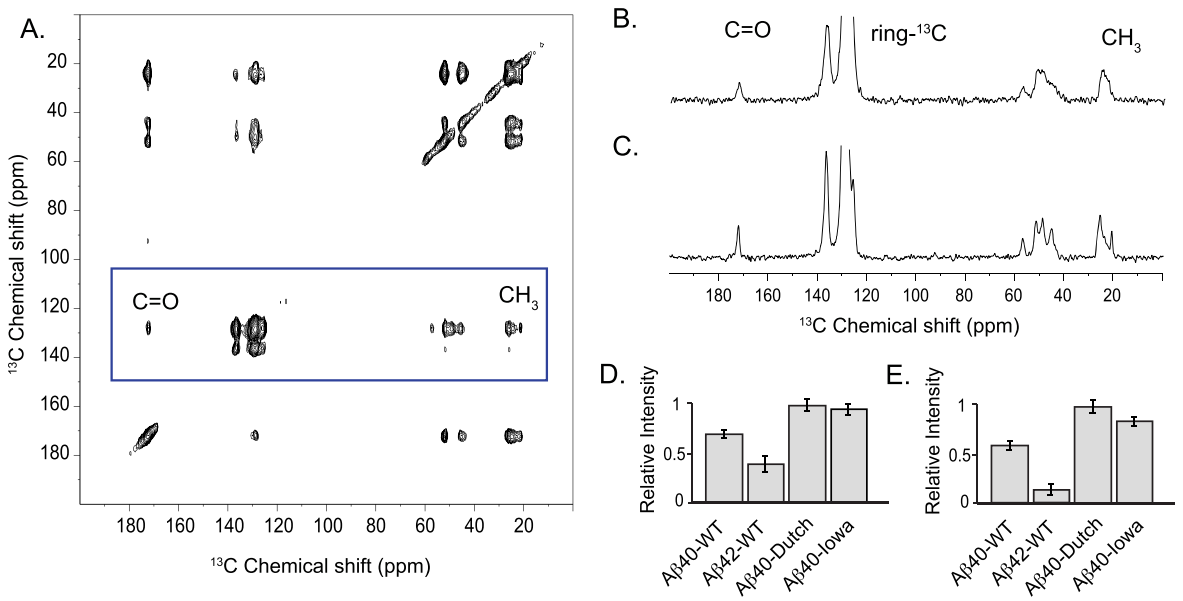

Figure 7. MAS NMR of Phe19−Leu34 contacts in Aβ monomers and fibrils of Aβ40-WT, Aβ40-Dutch, Aβ40-Iowa, and Aβ42-WT. (A) Two-dimensional ^{13}C DARR NMR spectrum of Aβ40-Iowa labeled with ring-^{13}C-Phe and U-^{13}C-Leu34. (B and C) Rows taken through the diagonal resonance of ring-^{13}C-Phe at time zero and 2 weeks, respectively, for Aβ40-Iowa. (D and E) Relative intensities of the ring-^{13}C-Phe−U-^{13}C-Leu34 cross peaks corresponding to the well-resolved Leu34 ^{13}C═O and $^{13}CH_3$ resonances at time zero and 2 weeks, respectively, relative to the ring-^{13}C-Phe diagonal resonance. The strongest cross-peak relative to the ring-^{13}C-Phe diagonal resonance was observed for Aβ40-Dutch, which was set equal to 1.0, at both time points. For the experiments using incubation for 2 weeks, the temperature was maintained at 37 °C. Errors shown are relative to the spectral noise.

MAS conditions, which in turn provides distance constraints between ^{13}C-labeled sites within the sample.

The 2D DARR NMR spectrum of Aβ40-Iowa fibrils containing ring-^{13}C-labeled Phe19 and uniformly ^{13}C-labeled Leu34 exhibits strong ^{13}C NMR resonances along the diagonal of the 2D NMR spectrum as well as strong off-diagonal cross-peaks (Figure 7A). The diagonal resonances are those that would appear in a one-dimensional NMR spectrum, whereas the off-diagonal cross peaks appear between ^{13}C sites that are separated by $\lesssim$6 Å. The 2D NMR spectrum in Figure 7A is of single-layer Aβ40-Iowa fibrils formed after 2 weeks at 37 °C. The cross-peaks observed between the resonances of ring-^{13}C-Phe19 and U-^{13}C-Leu34 indicate these residues are in close contact, in agreement with the structure of these fibrils.[37] Phe19 and Leu34 are found in close contact in the mature fibrils of Aβ40-WT but typically are not found in close association in fibril structures of Aβ42-WT.

Notably, the intense cross-peaks between Phe19 and Leu34 were also observed following monomerization of the Aβ40-Iowa peptide (see Experimental Section). Rows through the 2D NMR spectra at time zero (Figure 7B) and 2 weeks (Figure 7C) reveal the relative intensity between the diagonal resonance and cross-peaks. The cross-peaks in the spectrum obtained at time zero are much broader, which is consistent with a much more heterogeneous structure of the monomer compared to the fibrils formed after incubation for 2 weeks. For early time point experiments, monomeric Aβ was warmed to room temperature briefly before being rapidly frozen and lyophilized. The short time interval prior to measurement (or in this case before freezing) was similar to the initial time points at 25 °C for the SEC (Figure 2), FTIR (Figures 4 and 6), and AFM (Figure S2) measurements. Consequently, the samples contain a mixture of monomeric and oligomeric Aβ.

Measurements of Phe19−Leu34 interactions were also carried out on Aβ40-Dutch, Aβ40-WT, and Aβ42-WT in a similar fashion. The relative intensities of the ring-^{13}C-Phe19 and U-^{13}C-Leu34 cross-peaks relative to the Phe19 diagonal resonance are plotted for time zero (Figure 7D) and 2 weeks (Figure 7E). The cross-peak intensities for Aβ40-Dutch at time zero are comparable to those for Aβ40-Iowa, consistent with the strong antiparallel signature in the FTIR spectra at this initial time point for these two peptides. Cross-peaks with similar intensity are observed at both the time zero and 2 week time points. Dilution experiments (data not shown) indicate that these result from intramolecular interactions at time zero for Aβ40-Dutch and Aβ40-Iowa, but are intermolecular for Aβ40-Dutch and intramolecular for Aβ40-Iowa at the two week time point. The cross-peak intensities are markedly lower for Aβ40-WT at both time points than for the mutant peptides.

For Aβ42-WT, cross-peak intensity is observed at time zero, consistent with earlier observations for this interaction in Aβ42-WT oligomers.[69] However, the Phe−Leu cross-peak intensity drops at the 2 week time point after fibrils have formed, which is consistent with NMR and cryo-EM structures of Aβ42-WT fibrils.

Taken together, the observation of Phe−Leu contacts at time zero in all four peptides is consistent with the FTIR results suggesting rapid β-hairpin formation (Figures 4 and 5). The strong cross-peak intensity observed for the Aβ40-Dutch and Aβ40-Iowa peptides relative to Aβ40-WT and Aβ42-WT at the early time point correlates with the strong ~1611 cm^{-1} IR band characteristic of antiparallel β-hairpin structure.

DISCUSSION

CAA is a common disease in the aging population associated with cognitive decline and cerebral vascular compromise as a result of Aβ peptide deposition.[14,72] Although often present in

https://doi.org/10.1021/acs.biochem.1c00781
Biochemistry 2022, 61, 1181−1198

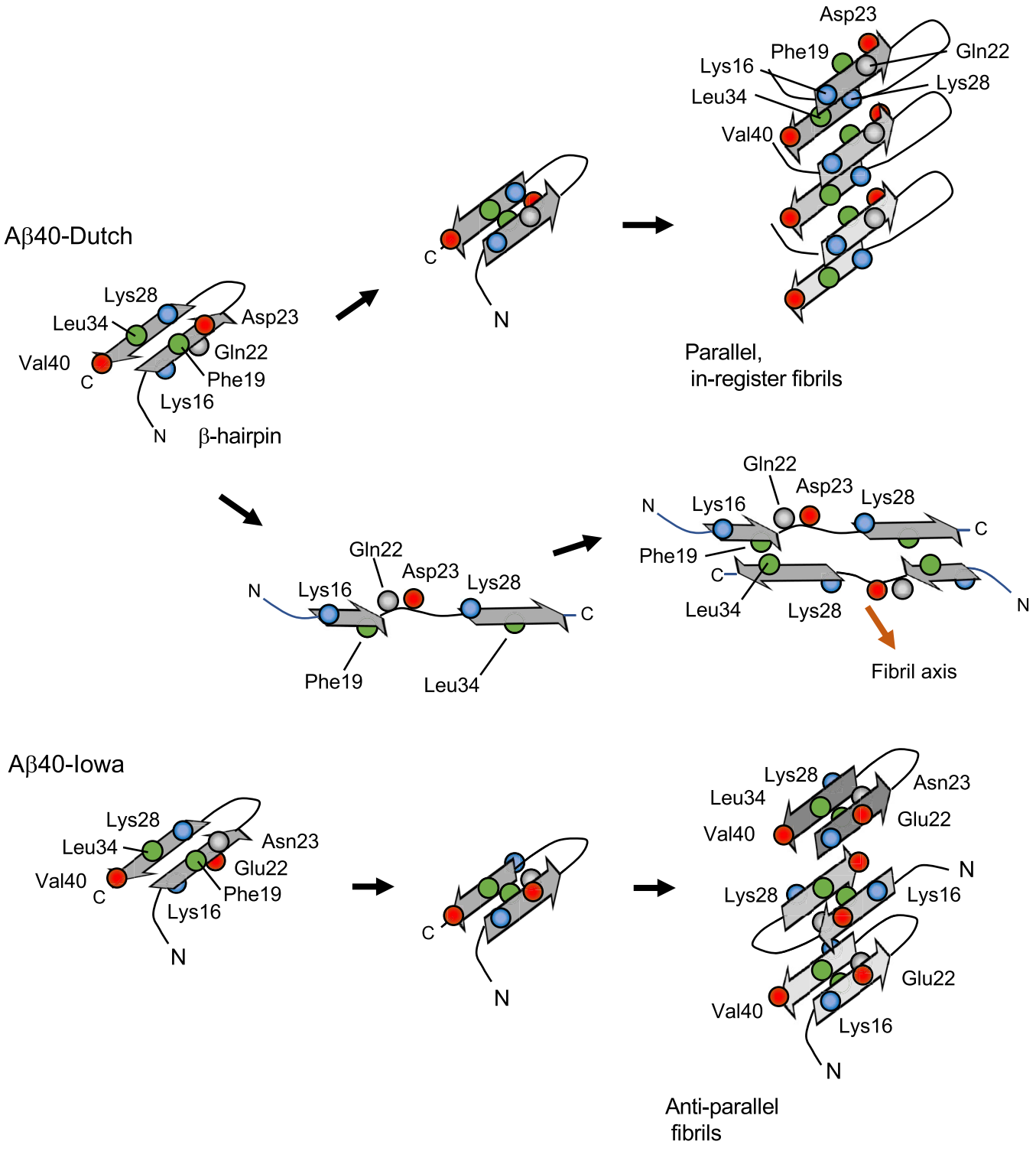

Figure 8. Conversion of β-hairpin to parallel, in-register, and antiparallel fibrils for Aβ40-Dutch and Aβ40-Iowa. β-Hairpin secondary structure is formed by association of two β-strands within the Aβ peptide and is stabilized by intramolecular hydrogen bonding, hydrophobic packing interactions, and complementary electrostatic interactions. Both FTIR and NMR measurements indicate that Aβ40-Dutch and Aβ40-Iowa peptides have a strong propensity for forming β-hairpin secondary structure as the first step in the pathway to fibrils. The NMR measurements show that Phe19 and Leu34 pack against each other on the same surface of the hairpin. These CAA familial mutant peptides have a higher propensity for β-hairpin compared to that of Aβ40-WT, which is attributed to the single complementary electrostatic interaction between Lys28 and either Glu22 (in Iowa) or Asp23 (in Dutch). Hydrogen bonding between β-strands switches from intramolecular to intermolecular in the transition from β-hairpin to cross β-sheet fibrils. A simple rotation of the β-strands to place the hydrophobic side chains in the center of a U-shaped structure (in Aβ40-Iowa and in the top pathway for Aβ40-Dutch) forms a nucleus for polymerization of additional monomers. In the antiparallel fibril structure of Aβ40-Iowa, the charged residues alternate along the fibril surface and provide stabilizing interactions. Disruption of the intramolecular interactions in the β-hairpin in Aβ40-Dutch causes unraveling of the peptide (bottom pathway). Addition of monomers to this structure would lead to a fibril structure similar to that observed for Aβ40-WT by Tycko and co-workers in human brain.[76]

https://doi.org/10.1021/acs.biochem.1c00781
Biochemistry 2022, 61, 1181−1198

AD cases, CAA has a distinct pathology. We focus on the Aβ40-Dutch (E22Q) and Aβ40-Iowa (D23N) peptides that are associated with familial forms of CAA. These peptides present similar mutations at neighboring positions in the Aβ sequence that turn an acidic amino acid into an uncharged amine, yet they are associated with distinct CAA subtypes. Aβ40-Dutch (E22Q) is associated with CAA type 2 and preferentially forms vascular amyloid on large cerebral vessels, while Aβ40-Iowa (D23N) is associated with CAA type 1 and preferentially aggregates on cerebral capillaries. We compare the solution properties of these two peptides to determine whether structural differences may account for differences in the sites of vascular deposition. We also compare these peptides with Aβ40-WT and Aβ42-WT, which have been more extensively characterized and appear to be preferentially associated with CAA type 2 and CAA type 1, respectively.

The Aβ40-Dutch and Aβ40-Iowa peptides were found to exhibit several differences *in vitro*, including the kinetics of fibril formation and the stabilities of the initial protofibrils or fibrils formed. While both peptides rapidly form β-hairpin structures, a key difference is that Aβ40-Dutch forms parallel, in-register fibrils while Aβ40-Iowa has a propensity to form single-layer antiparallel fibrils in the absence of strong agitation or sonication. We discuss the similarities and differences between these two peptides in terms of potential mechanisms of amyloid fibril formation, sites of vascular deposition, and clearance from the brain.

Propensity to Form Antiparallel β-Hairpin Structure in Solution. Aβ peptides can form two distinct antiparallel structures during the transition to mature fibrils. The first type of structure is an antiparallel β-hairpin, which in the studies described above is formed through intramolecular hydrogen bonding between the two hydrophobic stretches that form β-strands (Figure 8). The second antiparallel structure corresponds to fibrils with antiparallel cross β-sheet (discussed in the next section). In the latter, intermolecular hydrogen bonding occurs between β-strands from adjacent monomers within the fibril.

There are multiple lines of evidence for the formation of antiparallel β-hairpin structure in monomeric or oligomeric Aβ40-WT and Aβ42-WT. The $^{1}H-^{15}N$ HSQC studies of Hoshino and co-workers[59] described above concluded that chemical exchange occurs between random coil and β-hairpin structure in Aβ40-WT on the basis of the absence of a concentration dependence. This observation supports the conclusion that intramolecular conformational changes are responsible for the loss of NMR intensity with an increase in temperature. Intramolecular interactions are supported by cross-linking studies.[73,74] Aβ40-WT and Aβ42-WT peptides with intramolecular cross-links both spontaneously form stable oligomers and protofibrils, but both are unable to convert into amyloid fibrils. Conformation-specific antibodies used to detect Aβ aggregates *in vivo* indicate that the wild-type oligomer structure is preserved and stabilized in the cross-linked oligomers. Stabilization of a β-hairpin conformation was also found in monomeric Aβ40-WT bound to an affibody protein.[75] Finally, solid-state NMR studies have detected the formation of transient antiparallel β-hairpins prior to fibril formation.[48,71]

In the studies described above, the β-hairpins contain a turn between Asp23 and Lys28. The hydrophobic N-terminal β-strand of the β-hairpin comprises roughly residues Leu17–Ala21, while the hydrophobic C-terminal β-strand stretches at least from Ile31 to Val36. In addition to the intramolecular hydrogen bonding between β-strands, lateral packing of hydrophobic side chains provides stabilizing interactions. In addition to hydrophobic contacts within these stretches, complementary charges at the ends of the β-strands may contribute to electrostatic stabilization. For example, in the Aβ40-Dutch peptide, Lys28 may pair with Asp23 and Lys16 may pair with the C-terminal carboxyl of Val40 (Figure 8).

In our current studies, we address whether β-hairpins form in the Aβ40-Dutch and Aβ40-Iowa peptides in a fashion similar to that of Aβ40-WT. In the FTIR spectra of the Aβ40-Dutch and Aβ40-Iowa monomers and/or small oligomers, we observe much greater intensity in the low-frequency 1610–1612 cm^{-1} band (corresponding to antiparallel β-structure) in the mutant peptides compared to Aβ40-WT. Moreover, at the monomer/oligomer stage, intramolecular NMR contacts are observed between Phe19 and Leu34 in the Aβ40-Dutch and Aβ40-Iowa peptides that are consistent with an antiparallel β-hairpin structure involving the central hydrophobic Leu17-Val18-Phe19-Phe20-Ala21 sequence and the C-terminal Ile31-Val32-Gly33-Leu34-Met35-Val36 sequence (Figure 8). The exposed hydrophobic surfaces in these transiently formed structures may drive their association into oligomers and subsequent transition into fibrils. The β-hairpin structure shown in Figure 8 is consistent with previous solid-state NMR experiments of Aβ40-WT showing close contacts of Glu22 and Ile31 in early oligomeric or protofibril intemediates that are lost in the formation of mature fibrils.[71]

The rapid formation of the β-hairpin structure in Aβ40-Dutch and Aβ40-Iowa relative to Aβ40 and Aβ42 is one of the main features that these familial Aβ mutants have in common in terms of their solution properties. The SEC traces along with the corresponding TEM micrographs show that both peptides form fibrils rapidly under the temperature and slow shaking conditions used. The β-hairpins are likely a common initial stage in forming the nuclei that can seed fibril growth.[73,74] Also, a recent cryo-EM structure of brain-derived Aβ40-WT fibrils indicates that monomers adopting β-hairpin structure may associate with the fibril surface.[76] This observation raises the intriguing possibility that β-hairpin structure may be important for both fibril nucleation and fibril stability.

Correlation of Fibril Stability with CAA Type 1 and CAA Type 2. A growing body of evidence suggests that vascular amyloid deposition is associated with reduced peptide clearance[77,78] pointing to the clearance mechanism as a possible contributor to differences between CAA subtypes. Small cerebral vessels are sites of efflux across the blood–brain barrier and of perivascular drainage from the brain interstitial fluid.[79−81] We observed that Aβ40-Iowa and Aβ42-WT rapidly form stable protofibrils or fibrils at physiological temperature in the temperature-cycling NMR experiments, while less stable protofibrils or fibrils were observed for Aβ40-Dutch and Aβ40-WT. In the study presented here, we found that protofibril or fibril stability correlates best with the propensity of Aβ40-Iowa and Aβ42-WT to form vascular amyloid in CAA type 1 and Aβ40-Dutch and Aβ40-WT to form amyloid in CAA type 2.

Stable structures of Aβ40-Iowa and Aβ42-WT are less likely to cross cellular membrane barriers, which is required for transport out of the brain across the blood–brain barrier, or to drain along perivascular spaces, thus facilitating their deposition in capillaries. Conversely, less stable aggregates of Aβ40-WT or Aβ40-Dutch have a greater opportunity to

https://doi.org/10.1021/acs.biochem.1c00781
Biochemistry 2022, 61, 1181−1198

migrate along capillaries up the vascular tree through perivascular spaces, allowing fibrillar deposits to form in larger cerebral vessels. In addition, the differences in stability may also influence the ability of these peptides to interact with different isoforms of ApoE or other Aβ chaperones. In this regard, the ApoE4 allele has been linked to CAA type 1 while the ApoE2 and ApoE3 alleles are linked with CAA type 2.[14] ApoE4-Aβ complexes are less efficiently cleared across the blood−brain barrier through capillary endothelial cells than complexes of ApoE2-Aβ and ApoE3-Aβ,[82] suggesting a link between capillary deposition and a higher frequency of the ApoE4 allele.[14]

Propensity to Form Antiparallel Cross β-Sheet Fibril Structure in Solution. The second distinct type of antiparallel structure that can be formed by the Aβ peptides is an antiparallel fibril. Most structures of Aβ fibrils determined by NMR or cryo-EM have a parallel, in-register structure.[83] The Aβ40-Iowa peptide is unusual in forming single-layer fibrils that have elements similar to protofibrils. In the study presented here, we address whether Aβ40-Dutch has a similar propensity to form such structures. The FTIR studies in Figures 4 and 5 provide evidence that Aβ40-Dutch forms parallel fibrils upon incubation. While the FTIR spectra are similar at early time points between Aβ40-Dutch and Aβ40-Iowa, they are distinctly different at later times. The differences are confirmed by solid-state NMR measurements of Aβ40-Dutch and Aβ40-Iowa fibrils at the 2 week time point (Figure S6). While Aβ40-Iowa exhibits NMR contacts consistent with the single-layer antiparallel fibril structure, Aβ40-Dutch exhibits contacts consistent with parallel, in-register fibril structure.

One common element between the fibril structures of Aβ40-Iowa and Aβ42-WT (compared to Aβ40-WT and possibly Aβ40-Dutch) is the position of Lys28. In the single-layer fibril structure of Aβ40-Iowa, Tycko and co-workers[37] have previously shown that Asn23 is hydrogen bonded with Gln15 and Asn27. Lys28 is oriented outward (away from the fibril core) and forms a charge pair with the C-terminal carboxyl group on the neighboring peptide in the fibril. Glu22, the remaining negative charge, in the fibril core interacts with Lys16.

The fibril structures of Aβ42-WT that have a parallel, in-register orientation also show that Lys28 is oriented away from Glu22 or Asp23.[36,84] In these structures, Lys28 interacts electrostatically with the C-terminal carboxyl group at Ala42, resulting in a three-stranded β-sheet.

In contrast, in the fibril structures of Aβ40-WT, Asp23 and Lys28 typically form an intramolecular salt bridge.[85] The formation of this salt bridge appears to be the rate-determining step in fibril formation as it requires the Asp23 and Lys28 groups to rotate into the hydrophobic fibril core.[86] In the absence of such complementary charge matching, both residues prefer to be located on the surface of the fibril and solvated. However, mixtures of Aβ40-WT and Aβ42-WT can form unique fibril structures where Lys28 is oriented outward.[87] These studies indicate that even Aβ40-WT can form polymorphic structures in which the Asp23−Lys28 salt bridge is absent but more importantly suggest that the Aβ40-Iowa and Aβ42-WT peptides may be able to co-fibrillize in CAA type 1 vascular amyloid.

The Aβ40-Dutch peptide may form an Asp23−Lys28 salt bridge in a fashion similar to that of Aβ40-WT (Figure 8, top pathway). This orientation would be consistent with the strong NMR contact between ring-^{13}C-Phe19 and U-^{13}C-Leu34 observed in Figure 7. In both Aβ40-WT and Aβ40-Dutch, the NMR contact is intermolecular (data not shown). For Aβ40-WT formed in solution, this occurs due to staggering of β-strands between Aβ40 subunits. A second possible structure for Aβ40-Dutch is where both Gln22 and Asp23 remain oriented outward and are not in β-sheet or β-strand structure. Solid-state NMR studies of the E22G (Arctic)[88] and E22K (Italian) mutants of Aβ40[89] suggest polymorphism in their fibril structure. For E22K, NMR experiments have shown that the structural polymorphism reflects one population in which Asp23 has rotated inward to form a salt bridge with Lys28 and a second (major) population where the Asp23 side chain remains oriented outward and interacts electrostatically with the Lys22 side chain.[89]

One of the striking differences between Aβ40-Dutch and the three other Aβ peptides is the increase in intensity in the amide I region of the FTIR spectrum at ∼1670−1680 cm^{-1} in 10 mM NaCl (Figure 6C). This increase in intensity suggests that the β-hairpin unravels during the transition to mature fibrils. Unraveling would disrupt the hydrophobic interactions between the Leu17-Val18-Phe19-Phe20-Ala21 sequence in the middle of the Aβ peptide and the C-terminus (as shown in Figure 8, bottom pathway for Aβ40-Dutch fibrillization). Intermolecular association of these hydrophobic sequences would result in a fibril structure similar to the cryo-EM structure recently proposed by Tycko and co-workers.[76] This structure also exhibits intermolecular contacts between ring-^{13}C-Phe19 and U-^{13}C-Leu34.

Propensity to Form Antiparallel β-Structure in Human Brain. The Dutch E22Q and Iowa D23N mutations are relatively conservative changes that result in early onset and preferential deposition of vascular amyloid. One possibility is that the strong phenotypic influence that results from the mutation of a negatively charged residue to a neutral amine is due to the vascular membrane environment in which Aβ40-Dutch and Aβ40-Iowa form amyloid deposits. The measurements described here are under low-salt conditions that would favor electrostatic interactions, perhaps mimicking the role of membranes in excluding salt.

The Aβ40-Dutch and Aβ40-Iowa mutants preferentially form fibrils in the presence of the GM3 ganglioside, which is present on the surfaces of cerebral vascular smooth muscle cells.[90,91] Partitioning of the Aβ peptides into membranes may allow them to form antiparallel structures where the β-strands have complementary charge matching as observed in Aβ40-Iowa. We have shown that the antiparallel β-sheet structure in Aβ40-Iowa fibrils can be stabilized in solution with the addition of Cu^{2+},[47] a metal ion that is found to accumulate in vascular amyloid deposits. Moreover, we have recently observed antiparallel structure in fibrils derived from vascular amyloid isolated from human brain with sporadic CAA.[44] In these studies, templated growth of the brain-derived fibrils through multiple generations favors parallel, in-register β-sheet structure possibly due to the dilution of stabilizing cofactors such as Cu^{2+} or from the presence of less antiparallel β-hairpin that our current studies show rapidly forms when Aβ monomers are added to solution.

The residues at positions 22 and 23 may also contribute to electrostatic interactions that stabilize the N-terminus in structures of fibrils formed in vascular amyloid from Aβ40-WT. Cryo-EM structures suggest that fibrils derived from vascular amyloid may be quite different from parenchymal

https://doi.org/10.1021/acs.biochem.1c00781
Biochemistry 2022, 61, 1181−1198

amyloid.[92] In the structure reported by Kollmer et al.[92] of brain-derived Aβ40-WT from vascular amyloid, Glu22 and Asp23 interact near Asp1, resulting in a structured N-terminus formed by two antiparallel β-strands. The structure is similar to that of the C99 substrate prior to cleavage by γ-secretase.[93,94] In C99, membrane interactions appear to be responsible for stabilization of an N-terminal β-hairpin structure. Glu22 and Asp23 lie at the transition point of this N-terminal β-hairpin and the hydrophobic N-terminus, and consequently, they are at key positions for determining how the Aβ peptides generated by γ-secretase processing fold into fibrils. In this regard, the N-terminus, which is often observed to be unstructured in the structures of fibrils formed *in vitro*, may be a critical determinant of toxicity in the brain. For example, post-translational modifications involving N-terminal residues may play a role in fibril formation.[95] Recently, a novel β-hairpin fold of the N-terminus of Aβ has been used to generate antibodies that reduce the level of plaque formation in mouse of AD,[96] which may be similar to the target of aducanumab, an antibody that targets monomers and aggregated forms of Aβ.[97]

CONCLUSIONS

In summary, mutations in the Ala21-Glu22-Asn23 region have profound effects on the structure and phenotypic expression of the Aβ peptide. This region has been found to be a hot spot where mutations increase the level of fibril nucleation,[98] yet their phenotypic impacts can be quite different. In addition to E22Q and D23N, other mutations in this region include A21G (Flemish), E22K (Italian), and E22G (Arctic). For example, the D23N Iowa mutation is not associated with AD while the Arctic mutation is associated with AD and a high CAA type 1 load. The Dutch and Italian mutations are both associated with CAA type 2 and large lobar hemorrhages.[40] Nevertheless, pathological differences between patients with these familial mutants are not so "black and white" and often exhibit overlap. For instance, the Iowa mutation also leads in some cases to greater vessel deposition and hemorrhages, although less frequently than with the Dutch or Italian mutations. The variability between patients harboring the Iowa mutation could involve other factors. Aβ chaperones and the presence of both mutant and wild-type Aβ species in familial CAA patients heterozygous for the mutation may influence the assembly and deposition of vascular amyloid in different vascular beds.

Here we focus on the E22Q and D23N mutations that exhibit different phenotypes despite similar amino acid changes. Comparison of the two peptides in solution reveals both similar and strikingly different properties. Both Aβ40-Dutch and Aβ40-Iowa appear to rapidly form intramolecular β-hairpin structures consistent with their kinetics of fibril formation being faster than for Aβ40-WT. Aβ40-Dutch and Aβ40-WT, which are more prominent in CAA type 2, both form aggregates that are much less stable than Aβ40-Iowa and Aβ42-WT, which are favored in CAA type 1. Aβ40-Dutch and Aβ40-Iowa also differ strongly in their ability to form antiparallel β-sheet fibrils with Aβ40-Dutch preferentially forming parallel, in-register fibrils and Aβ40-Iowa forming extended antiparallel β-sheet protofibrils or single-layer fibrils (under the conditions studied). These properties in solution may be related to the ability of the different peptides to nucleate fibrils in vascular amyloid and/or be cleared from the brain parenchyma. Future studies correlating *in vitro* and *in vivo* properties promise to shed light on the familial mutations involving these residues.

ASSOCIATED CONTENT

Supporting Information

The Supporting Information is available free of charge at https://pubs.acs.org/doi/10.1021/acs.biochem.1c00781.

TEM and AFM images of the formation of Aβ42 protofibrils and fibrils, TEM and AFM images of the formation of Aβ40-Iowa protofibrils and fibrils, transition of Aβ40-WT and Aβ40-Iowa oligomers to fibrils by FTIR and TEM, model peptides that form antiparallel and parallel, in-register fibrils that illustrate the influence of 1-^{13}C labeling on the FTIR spectra, TEM image of Aβ42 showing a mixture of protofibrils and fibrils after incubation at 25 °C for 2 weeks, and overlaid FTIR spectra of Aβ40-WT, Aβ40-Dutch, Aβ40-Iowa, and Aβ42-WT at time zero, 3 h, and 2 weeks to better illustrate the intensity changes in the amide I region with and without LAGG ^{13}C labeling (PDF)

AUTHOR INFORMATION

Corresponding Author

Steven O. Smith − *Department of Biochemistry and Cell Biology, Center for Structural Biology, Stony Brook University, Stony Brook, New York 11794-5215, United States*; orcid.org/0000-0003-1861-7159; Email: steven.o.smith@stonybrook.edu

Authors

Jitika Rajpoot − *Department of Biochemistry and Cell Biology, Center for Structural Biology, Stony Brook University, Stony Brook, New York 11794-5215, United States*

Elliot J. Crooks − *Department of Biochemistry and Cell Biology, Center for Structural Biology, Stony Brook University, Stony Brook, New York 11794-5215, United States*; orcid.org/0000-0001-6062-0955

Brandon A. Irizarry − *Department of Biochemistry and Cell Biology, Center for Structural Biology, Stony Brook University, Stony Brook, New York 11794-5215, United States*

Ashley Amundson − *Department of Biochemistry and Cell Biology, Center for Structural Biology, Stony Brook University, Stony Brook, New York 11794-5215, United States*

William E. Van Nostrand − *George and Anne Ryan Institute for Neuroscience and Department of Biomedical and Pharmaceutical Sciences, University of Rhode Island, Kingston, Rhode Island 02881, United States*

Complete contact information is available at: https://pubs.acs.org/10.1021/acs.biochem.1c00781

Funding

This work was supported by National Institutes of Health Grants AG-27317 and NS-092696 (to S.O.S. and W.E.V.N.).

Notes

The authors declare no competing financial interest.

ACKNOWLEDGMENTS

The authors thank Martine Ziliox for assistance with the NMR measurements and critical review of the manuscript.

■ ABBREVIATIONS

Aβ, amyloid β; AD, Alzheimer's disease; CAA, cerebral amyloid angiopathy; DARR, dipolar-assisted rotational resonance; FTIR, Fourier transform infrared; HSQC, heteronuclear single-quantum correlation; MAS, magic angle spinning; NMR, nuclear magnetic resonance; SEC, size exclusion chromatography; TEM, transmission electron microscopy; WT, wild type.

■ REFERENCES

(1) Wolfe, M. S.; Xia, W. M.; Ostaszewski, B. L.; Diehl, T. S.; Kimberly, W. T.; Selkoe, D. J. Two transmembrane aspartates in presenilin-1 required for presenilin endoproteolysis and γ-secretase activity. *Nature* **1999**, *398*, 513−517.

(2) Scheuner, D.; Eckman, C.; Jensen, M.; Song, X.; Citron, M.; Suzuki, N.; Bird, T. D.; Hardy, J.; Hutton, M.; Kukull, W.; Larson, E.; LevyLahad, E.; Viitanen, M.; Peskind, E.; Poorkaj, P.; Schellenberg, G.; Tanzi, R.; Wasco, W.; Lannfelt, L.; Selkoe, D.; Younkin, S. Secreted amyloid β-protein similar to that in the senile plaques of Alzheimer's disease is increased in vivo by the presenilin 1 and 2 and APP mutations linked to familial Alzheimer's disease. *Nat. Med.* **1996**, *2*, 864−870.

(3) Iwatsubo, T.; Odaka, A.; Suzuki, N.; Mizusawa, H.; Nukina, N.; Ihara, Y. Visualization of Aβ42(43) and Aβ40 in senile plaques with end-specific Aβ monoclonals: Evidence that an initially deposited species is Aβ42(43). *Neuron* **1994**, *13*, 45−53.

(4) Kakuda, N.; Miyasaka, T.; Iwasaki, N.; Nirasawa, T.; Wada-Kakuda, S.; Takahashi-Fujigasaki, J.; Murayama, S.; Ihara, Y.; Ikegawa, M. Distinct deposition of amyloid-β species in brains with Alzheimer's disease pathology visualized with MALDI imaging mass spectrometry. *Acta Neuropathol. Commun.* **2017**, *5*, 73 DOI: 10.1186/s40478-017-0477-x.

(5) Borchelt, D. R.; Thinakaran, G.; Eckman, C. B.; Lee, M. K.; Davenport, F.; Ratovitsky, T.; Prada, C. M.; Kim, G.; Seekins, S.; Yager, D.; Slunt, H. H.; Wang, R.; Seeger, M.; Levey, A. I.; Gandy, S. E.; Copeland, N. G.; Jenkins, N. A.; Price, D. L.; Younkin, S. G.; Sisodia, S. S. Familial Alzheimer's disease-linked presenilin 1 variants elevate Aβ 1−42/1−40 ratio in vitro and in vivo. *Neuron* **1996**, *17*, 1005−1013.

(6) Charidimou, A.; Boulouis, G.; Gurol, M. E.; Ayata, C.; Bacskai, B. J.; Frosch, M. P.; Viswanathan, A.; Greenberg, S. M. Emerging concepts in sporadic cerebral amyloid angiopathy. *Brain* **2017**, *140*, 1829−1850.

(7) Thal, D. R.; Griffin, W. S. T.; de Vos, R. A. I.; Ghebremedhin, E. Cerebral amyloid angiopathy and its relationship to Alzheimer's disease. *Acta Neuropathol.* **2008**, *115*, 599−609.

(8) Auriel, E.; Greenberg, S. M. The pathophysiology and clinical presentation of cerebral amyloid angiopathy. *Curr. Athero. Rep.* **2012**, *14*, 343−350.

(9) Biffi, A.; Greenberg, S. M. Cerebral amyloid angiopathy: A systematic review. *J. Clin. Neuro.* **2011**, *7*, 1−9.

(10) Attems, J.; Jellinger, K.; Thal, D. R.; Van Nostrand, W. Sporadic cerebral amyloid angiopathy. *Neuropathol. Appl. Neurobiol.* **2011**, *37*, 75−93.

(11) Kalaria, R. N.; Ballard, C. Overlap between pathology of Alzheimer disease and vascular dementia. *Alzheimer Dis. Assoc. Disorders* **1999**, *13*, S115−S123.

(12) Jellinger, K. A. Alzheimer disease and cerebrovascular pathology: an update. *J. Neural Transm.* **2002**, *109*, 813−836.

(13) Brenowitz, W. D.; Nelson, P. T.; Besser, L. M.; Heller, K. B.; Kukull, W. A. Cerebral amyloid angiopathy and its co-occurrence with Alzheimer's disease and other cerebrovascular neuropathologic changes. *Neurobiol. Aging* **2015**, *36*, 2702−2708.

(14) Thal, D. R.; Ghebremedhin, E.; Rub, U.; Yamaguchi, H.; Del Tredici, K.; Braak, H. Two types of sporadic cerebral amyloid angiopathy. *J. Neuropath. Exp. Neuro.* **2002**, *61*, 282−293.

(15) Attems, J.; Lintner, F.; Jellinger, K. A. Amyloid β peptide 1−42 highly correlates with capillary cerebral amyloid angiopathy and Alzheimer disease pathology. *Acta Neuropathol.* **2004**, *107*, 283−291.

(16) Oshima, K.; Akiyama, H.; Tsuchiya, K.; Kondo, H.; Haga, C.; Shimomura, Y.; Iseki, E.; Uchikado, H.; Kato, M.; Niizato, K.; Arai, H. Relative paucity of tau accumulation in the small areas with abundant Aβ42-positive capillary amyloid angiopathy within a given cortical region in the brain of patients with Alzheimer pathology. *Acta Neuropathol.* **2006**, *111*, 510−518.

(17) Rebeck, G. W.; Cho, H. S.; Grabowski, T. J.; Greenberg, S. M. The effects of AβPP mutations and APOE polymorphisms on cerebral amyloid angiopathy. *Amyloid* **2001**, *8*, 43−47.

(18) Akiyama, H.; Mori, H.; Sahara, N.; Kondo, H.; Ikeda, K.; Nishimura, T.; Oda, T.; McGeer, P. L. Variable deposition of amyloid β-protein (Aβ) with the carboxy-terminus that ends at residue valine(40) (Aβ40) in the cerebral cortex of patients with Alzheimer's disease: A double-labeling immunohistochemical study with antibodies specific for Aβ40 and the Aβ that ends at residues alanine(42)/threonine(43) (Aβ42). *Neurochem. Res.* **1997**, *22*, 1499−1506.

(19) Miao, J. T.; Vitek, M. P.; Xu, F.; Previti, M. L.; Davis, J.; Van Nostrand, W. E. Reducing cerebral microvascular amyloid-β protein deposition diminishes regional neuroinflammation in vasculotropic mutant amyloid precursor protein transgenic mice. *J. Neurosci.* **2005**, *25*, 6271−6277.

(20) Miao, J.; Xu, F.; Davis, J.; Otte-Holler, I.; Verbeek, M. M.; Van Nostrand, W. E. Cerebral microvascular amyloid-β protein deposition induces vascular degeneration and neuroinflammation in transgenic mice expressing human vasculotropic mutant amyloid beta precursor protein. *Am. J. Pathol.* **2005**, *167*, 505−515.

(21) Zhu, X. Y.; Hatfield, J.; Sullivan, J. K.; Xu, F.; Van Nostrand, W. E. Robust neuroinflammation and perivascular pathology in rTg-DI rats, a novel model of microvascular cerebral amyloid angiopathy. *J. Neuroinflammation* **2020**, *17*, 78 DOI: 10.1186/s12974-020-01755-y.

(22) van Duinen, S. G.; Castano, E. M.; Prelli, F.; Bots, G. T.; Luyendijk, W.; Frangione, B. Hereditary cerebral hemorrhage with amyloidosis in patients of Dutch origin is related to Alzheimer disease. *Proc. Natl. Acad. Sci. U.S.A.* **1987**, *84*, 5991−5994.

(23) Wattendorff, A. R.; Frangione, B.; Luyendijk, W.; Bots, G. T. A. M. Hereditary cerebral haemorrhage with amyloidosis, Dutch type (HCHWA-D): clinicopathological studies. *J. Neuro. Neurosurg. Psych.* **1995**, *58*, 699−705.

(24) Maat-Schieman, M. L.; van Duinen, S. G.; Rozemuller, A. J.; Haan, J.; Roos, R. A. Association of vascular amyloid β and cells of the mononuclear phagocyte system in hereditary cerebral hemorrhage with amyloidosis (Dutch) and Alzheimer disease. *J. Neuropathol. Exp. Neurol.* **1997**, *56*, 273−284.

(25) Maat-Schieman, M. L.; Yamaguchi, H.; Hegeman-Kleinn, I. M.; Welling-Graafland, C.; Natté, R.; Roos, R. A.; van Duinen, S. G. Glial reactions and the clearance of amyloid β protein in the brains of patients with hereditary cerebral hemorrhage with amyloidosis-Dutch type. *Acta Neuropathol.* **2004**, *107*, 389−398.

(26) Rozemuller, A. J.; Roos, R. A.; Bots, G. T.; Kamphorst, W.; Eikelenboom, P.; Van Nostrand, W. E. Distribution of β/A4 protein and amyloid precursor protein in hereditary cerebral hemorrhage with amyloidosis-Dutch type and Alzheimer's disease. *Am. J. Pathol.* **1993**, *142*, 1449−1457.

(27) Grabowski, T. J.; Cho, H. S.; Vonsattel, J. P.; Rebeck, G. W.; Greenberg, S. M. Novel amyloid precursor protein mutation in an Iowa family with dementia and severe cerebral amyloid angiopathy. *Ann. Neurol.* **2001**, *49*, 697−705.

(28) Shin, Y.; Cho, H. S.; Rebeck, G. W.; Greenberg, S. M. Vascular changes in Iowa-type hereditary cerebral amyloid angiopathy. *Ann. N.Y. Acad. Sci.* **2002**, *977*, 245−251.

(29) Levy, E.; Carman, M. D.; Fernandez-Madrid, I. J.; Power, M. D.; Lieberburg, I.; van Duinen, S. G.; Bots, G. T.; Luyendijk, W.; Frangione, B. Mutation of the Alzheimer's disease amyloid gene in hereditary cerebral hemorrhage, Dutch type. *Science* **1990**, *248*, 1124−1126.

https://doi.org/10.1021/acs.biochem.1c00781
Biochemistry 2022, 61, 1181−1198

(30) Van Broeckhoven, C.; Haan, J.; Bakker, E.; Hardy, J. A.; Van Hul, W.; Wehnert, A.; Vegter-Van der Vlis, M.; Roos, R. A. Amyloid β protein precursor gene and hereditary cerebral hemorrhage with amyloidosis (Dutch). *Science* **1990**, *248*, 1120−1122.
(31) Rutgers, K. S.; van Remoortere, A.; van Buchem, M. A.; Verrips, C. T.; Greenberg, S. M.; Bacskai, B. J.; Frosch, M. P.; van Duinen, S. G.; Maat-Schieman, M. L.; van der Maarel, S. M. Differential recognition of vascular and parenchymal β amyloid deposition. *Neuro. Aging* **2011**, *32*, 1774−1783.
(32) Han, B. H.; Zhou, M. L.; Vellimana, A. K.; Milner, E.; Kim, D. H.; Greenberg, J. K.; Chu, W. H.; Mach, R. H.; Zipfel, G. J. Resorufin analogs preferentially bind cerebrovascular amyloid: potential use as imaging ligands for cerebral amyloid angiopathy. *Mol. Neurodegener.* **2011**, *6*, 86.
(33) Benzinger, T. L. S.; Gregory, D. M.; Burkoth, T. S.; Miller-Auer, H.; Lynn, D. G.; Botto, R. E.; Meredith, S. C. Propagating structure of Alzheimer's β-amyloid(10−35) is parallel β-sheet with residues in exact register. *Proc. Natl. Acad. Sci. U.S.A.* **1998**, *95*, 13407−13412.
(34) Petkova, A. T.; Leapman, R. D.; Guo, Z. H.; Yau, W. M.; Mattson, M. P.; Tycko, R. Self-propagating, molecular-level polymorphism in Alzheimer's β-amyloid fibrils. *Science* **2005**, *307*, 262−265.
(35) Tycko, R. Solid-state NMR studies of amyloid fibril structure. *Annu. Rev. Phys. Chem.* **2011**, *62*, 279−299.
(36) Gremer, L.; Scholzel, D.; Schenk, C.; Reinartz, E.; Labahn, J.; Ravelli, R. B. G.; Tusche, M.; Lopez-Iglesias, C.; Hoyer, W.; Heise, H.; Willbold, D.; Schroder, G. F. Fibril structure of amyloid-β (1−42) by cryo-electron microscopy. *Science* **2017**, *358*, 116−119.
(37) Qiang, W.; Yau, W.-M.; Luo, Y.; Mattson, M. P.; Tycko, R. Antiparallel β-sheet architecture in Iowa-mutant β-amyloid fibrils. *Proc. Natl. Acad. Sci. U.S.A.* **2012**, *109*, 4443−4448.
(38) Sgourakis, N. G.; Yau, W. M.; Qiang, W. Modeling an in-register, parallel "Iowa" Aβ fibril structure using solid-state NMR data from labeled samples with rosetta. *Structure* **2015**, *23*, 216−227.
(39) Fu, Z.; Van Nostrand, W. E.; Smith, S. O. Anti-parallel β-hairpin structure in soluble Aβ oigomers of Aβ40-Dutch and Aβ40-Iowa. *Int. J. Mol. Sci.* **2021**, *22*, 1225.
(40) Kumar-Singh, S. Hereditary and sporadic forms of Aβ-cerebrovascular amyloidosis and relevant transgenic mouse models. *Int. J. Mol. Sci.* **2009**, *10*, 1872−1895.
(41) Hubin, E.; Deroo, S.; Schierle, G. K.; Kaminski, C.; Serpell, L.; Subramaniam, V.; van Nuland, N.; Broersen, K.; Raussens, V.; Sarroukh, R. Two distinct β-sheet structures in Italian-mutant amyloid-β fibrils: a potential link to different clinical phenotypes. *Cell. Mol. Life Sci.* **2015**, *72*, 4899−4913.
(42) Xu, F.; Fu, Z.; Dass, S.; Kotarba, A. E.; Davis, J.; Smith, S. O.; Van Nostrand, W. E. Cerebral vascular amyloid seeds drive amyloid β-protein fibril assembly with a distinct anti-parallel structure. *Nature Comm.* **2016**, *7*, 13527.
(43) Davis, J.; Xu, F.; Hatfield, J.; Lee, H.; Hoos, M. D.; Popescu, D.; Crooks, E.; Kim, R.; Smith, S. O.; Robinson, J. K.; Benveniste, H.; Van Nostrand, W. E. A novel transgenic rat model of robust cerebral microvascular amyloid with prominent vasculopathy. *Am. J. Pathol.* **2018**, *188*, 2877−2889.
(44) Irizarry, B. A.; Davis, J.; Zhu, X.; Boon, B. D. C.; Rozemuller, A. J.; Van Nostrand, W. E.; Smith, S. O. Human cerebral vascular amyloid contains both anti-parallel and parallel in-register Aβ40 fibrils. *J. Biol. Chem.* **2021**, *297*, 101259.
(45) Attems, J.; Jellinger, K. A. Only cerebral capillary amyloid angiopathy correlates with Alzheimer pathology–a pilot study. *Acta Neuropathol.* **2004**, *107*, 83−90.
(46) Bornebroek, M.; De Jonghe, C.; Haan, J.; Kumar-Singh, S.; Younkin, S.; Roos, R.; Van Broeckhoven, C. Hereditary cerebral hemorrhage with amyloidosis Dutch type (AβPP 693): decreased plasma amyloid-β 42 concentration. *Neurobiol. Dis.* **2003**, *14*, 619−623.
(47) Crooks, E. J.; Irizarry, B. A.; Ziliox, M.; Kawakami, T.; Victor, T.; Xu, F.; Hojo, H.; Chiu, K.; Simmerling, C.; Van Nostrand, W. E.; Smith, S. O.; Miller, L. M. Copper stabilizes antiparallel β-sheet fibrils of the amyloid-β40 (Aβ40)-Iowa variant. *J. Biol. Chem.* **2020**, *295*, 8914−8927.
(48) Fu, Z.; Aucoin, D.; Davis, J.; Van Nostrand, W. E.; Smith, S. O. Mechanism of nucleated conformational conversion of Aβ42. *Biochemistry* **2015**, *54*, 4197−4207.
(49) Lee, C. F.; Bird, S.; Shaw, M.; Jean, L.; Vaux, D. J. Combined effects of agitation, macromolecular crowding, and interfaces on amyloidogenesis. *J. Biol. Chem.* **2012**, *287*, 38006−38019.
(50) Fitzpatrick, A. W. P.; Falcon, B.; He, S.; Murzin, A. G.; Murshudov, G.; Garringer, H. J.; Crowther, R. A.; Ghetti, B.; Goedert, M.; Scheres, S. H. W. Cryo-EM structures of tau filaments from Alzheimer's disease. *Nature* **2017**, *547*, 185−190.
(51) Takegoshi, K.; Nakamura, S.; Terao, T. ^{13}C-^{1}H dipolar-assisted rotational resonance in magic-angle spinning NMR. *Chem. Phys. Lett.* **2001**, *344*, 631−637.
(52) Van Nostrand, W. E.; Melchor, J. P.; Cho, H. S.; Greenberg, S. M.; Rebeck, G. W. Pathogenic effects of D23N Iowa mutant amyloid β-protein. *J. Biol. Chem.* **2001**, *276*, 32860−32866.
(53) Hatami, A.; Monjazeb, S.; Milton, S.; Glabe, C. G. Familial Alzheimer's disease mutations within the amyloid precursor protein alter the aggregation and conformation of the amyloid-β peptide. *J. Biol. Chem.* **2017**, *292*, 3172−3185.
(54) Bitan, G.; Kirkitadze, M. D.; Lomakin, A.; Vollers, S. S.; Benedek, G. B.; Teplow, D. B. Amyloid β-protein (Aβ) assembly: Aβ40 and Aβ42 oligomerize through distinct pathways. *Proc. Natl. Acad. Sci. U.S.A.* **2003**, *100*, 330−335.
(55) Fu, Z.; Aucoin, D.; Ahmed, M.; Ziliox, M.; Van Nostrand, W. E.; Smith, S. O. Capping of Aβ42 oligomers by small molecule inhibitors. *Biochemistry* **2014**, *53*, 7893−7903.
(56) Nilsberth, C.; Westlind-Danielsson, A.; Eckman, C. B.; Condron, M. M.; Axelman, K.; Forsell, C.; Stenh, C.; Luthman, J.; Teplow, D. B.; Younkin, S. G.; Naslund, J.; Lannfelt, L. The 'Arctic' APP mutation (E693G) causes Alzheimer's disease by enhanced Aβ protofibril formation. *Nat. Neurosci.* **2001**, *4*, 887−893.
(57) Johansson, A. S.; Berglind-Dehlin, F.; Karlsson, G.; Edwards, K.; Gellerfors, P.; Lannfelt, L. Physiochemical characterization of the Alzheimer's disease-related peptides Aβ1−42Arctic and Aβ1−42wt. *FEBS J.* **2006**, *273*, 2618−2630.
(58) Fawzi, N. L.; Ying, J. F.; Torchia, D. A.; Clore, G. M. Kinetics of amyloid β monomer-to-oligomer exchange by NMR relaxation. *J. Am. Chem. Soc.* **2010**, *132*, 9948−9951.
(59) Yamaguchi, T.; Matsuzaki, K.; Hoshino, M. Transient formation of intermediate conformational states of amyloid-β peptide revealed by heteronuclear magnetic resonance spectroscopy. *FEBS Lett.* **2011**, *585*, 1097−1102.
(60) Fawzi, N. L.; Ying, J.; Ghirlando, R.; Torchia, D. A.; Clore, G. M. Atomic-resolution dynamics on the surface of amyloid-β protofibrils probed by solution NMR. *Nature* **2011**, *480*, 268−272.
(61) Flynn, J. D.; Jiang, Z. P.; Lee, J. C. Segmental C-13-labeling and Raman microspectroscopy of alpha-synuclein amyloid formation. *Angew. Chem.-Int. Ed.* **2018**, *57*, 17069−17072.
(62) Cerf, E.; Sarroukh, R.; Tamamizu-Kato, S.; Breydo, L.; Derclaye, S.; Dufrene, Y. F.; Narayanaswami, V.; Goormaghtigh, E.; Ruysschaert, J. M.; Raussens, V. Antiparallel β-sheet: a signature structure of the oligomeric amyloid β-peptide. *Biochem. J.* **2009**, *421*, 415−423.
(63) Gu, L.; Liu, C.; Stroud, J. C.; Ngo, S.; Jiang, L.; Guo, Z. Antiparallel triple-strand architecture for prefibrillar Aβ42 oligomers. *J. Biol. Chem.* **2014**, *289*, 27300−27313.
(64) Paul, C.; Wang, J. P.; Wimley, W. C.; Hochstrasser, R. M.; Axelsen, P. H. Vibrational coupling, isotopic editing, and β-sheet structure in a membrane-bound polypeptide. *J. Am. Chem. Soc.* **2004**, *126*, 5843−5850.
(65) Petty, S. A.; Decatur, S. M. Experimental evidence for the reorganization of β-strands within aggregates of the Aβ(16−22) peptide. *J. Am. Chem. Soc.* **2005**, *127*, 13488−13489.
(66) Goto, Y.; Adachi, M.; Muta, H.; So, M. Salt-induced formations of partially folded intermediates and amyloid fibrils suggests a common underlying mechanism. *Biophys. Rev.* **2018**, *10*, 493−502.

https://doi.org/10.1021/acs.biochem.1c00781
Biochemistry 2022, 61, 1181−1198

(67) Klement, K.; Wieligmann, K.; Meinhardt, J.; Hortschansky, P.; Richter, W.; Fandrich, M. Effect of different salt ions on the propensity of aggregation and on the structure of Alzheimer's Aβ (1−40) amyloid fibrils. *J. Mol. Biol.* **2007**, *373*, 1321−1333.
(68) Shea, D.; Hsu, C. C.; Bi, T. M.; Paranjapye, N.; Childers, M. C.; Cochran, J.; Tomberlin, C. P.; Wang, L. B.; Paris, D.; Zonderman, J.; Varani, G.; Link, C. D.; Mullan, M.; Daggett, V. alpha-Sheet secondary structure in amyloid β-peptide drives aggregation and toxicity in Alzheimer's disease. *Proc. Natl. Acad. Sci. U.S.A.* **2019**, *116*, 8895−8900.
(69) Ahmed, M.; Davis, J.; Aucoin, D.; Sato, T.; Ahuja, S.; Aimoto, S.; Elliott, J. I.; Van Nostrand, W. E.; Smith, S. O. Structural conversion of neurotoxic amyloid-β_{1-42} oligomers to fibrils. *Nat. Struct. Mol. Biol.* **2010**, *17*, 561−567.
(70) Das, A. K.; Rawat, A.; Bhowmik, D.; Pandit, R.; Huster, D.; Maiti, S. An early folding contact between Phe19 and Leu34 is critical for amyloid-β oligomer toxicity. *ACS Chem. Neurosci.* **2015**, *6*, 1290−1295.
(71) Scheidt, H. A.; Morgado, I.; Huster, D. Solid-state NMR reveals a close structural relationship between amyloid-β protofibrils and oligomers. *J. Biol. Chem.* **2012**, *287*, 22822−22826.
(72) Greenberg, S. M.; Bacskai, B. J.; Hernandez-Guillamon, M.; Pruzin, J.; Sperling, R.; van Veluw, S. J. Cerebral amyloid angiopathy and Alzheimer's disease - one peptide, two pathways. *Nature Rev. Neuro.* **2020**, *16*, 30−42.
(73) Sandberg, A.; Luheshi, L. M.; Sollvander, S.; Pereira de Barros, T.; Macao, B.; Knowles, T. P. J.; Biverstal, H.; Lendel, C.; Ekholm-Petterson, F.; Dubnovitsky, A.; Lannfelt, L.; Dobson, C. M.; Hard, T. Stabilization of neurotoxic Alzheimer amyloid-β oligomers by protein engineering. *Proc. Natl. Acad. Sci. U. S. A.* **2010**, *107*, 15595−15600.
(74) Hard, T. Protein engineering to stabilize soluble amyloid β-protein aggregates for structural and functional studies. *FEBS J.* **2011**, *278*, 3884−3892.
(75) Hoyer, W.; Gronwall, C.; Jonsson, A.; Stahl, S.; Hard, T. Stabilization of a beta-hairpin in monomeric Alzheimer's amyloid-β peptide inhibits amyloid formation. *Proc. Natl. Acad. Sci. U.S.A.* **2008**, *105*, 5099−5104.
(76) Ghosh, U.; Thurber, K. R.; Yau, W. M.; Tycko, R. Molecular structure of a prevalent amyloid-β fibril polymorph from Alzheimer's disease brain tissue. *Proc. Natl. Acad. Sci. U.S.A.* **2021**, *118*, e2023089118 DOI: 10.1073/pnas.2023089118.
(77) Deane, R.; Bell, R. D.; Sagare, A.; Zlokovic, B. V. Clearance of amyloid-beta peptide Across the blood-brain barrier: Implication for therapies in Alzheimer's disease. *CNS Neurol. Disord. Drug Targets* **2009**, *8*, 16−30.
(78) Mawuenyega, K. G.; Sigurdson, W.; Ovod, V.; Munsell, L.; Kasten, T.; Morris, J. C.; Yarasheski, K. E.; Bateman, R. J. Decreased clearance of CNS β-amyloid in Alzheimer's disease. *Science* **2010**, *330*, 1774−1774.
(79) Zlokovic, B. V. Neurovascular pathways to neurodegeneration in Alzheimer's disease and other disorders. *Nature Rev. Neurosci.* **2011**, *12*, 723−738.
(80) Weller, R. O.; Massey, A.; Newman, T. A.; Hutchincs, M.; Kuo, Y. M.; Roher, A. Amyloid angiopathy and the perivascular drainage of β-amyloid from the human brain. *J. Neuropathol. Exp. Neurol.* **1998**, *57*, 471−471.
(81) Marin-Padilla, M.; Knopman, D. S. Developmental aspects of the intracerebral microvasculature and perivascular spaces: Insights into brain response to late-life diseases. *J. Neuropath. Exp. Neuro.* **2011**, *70*, 1060−1069.
(82) Deane, R.; Sagare, A.; Hamm, K.; Parisi, M.; Lane, S.; Finn, M. B.; Holtzman, D. M.; Zlokovic, B. V. apoE isoform-specific disruption of amyloid β peptide clearance from mouse brain. *J. Clin. Invest.* **2008**, *118*, 4002−4013.
(83) Toyama, B. H.; Weissman, J. S. Amyloid structure: Conformational diversity and consequences. *Annu. Rev. Biochem.* **2011**, *80*, 557−585.
(84) Xiao, Y.; Ma, B.; McElheny, D.; Parthasarathy, S.; Long, F.; Hoshi, M.; Nussinov, R.; Ishii, Y. Aβ(1−42) fibril structure illuminates self-recognition and replication of amyloid in Alzheimer's disease. *Nat. Struct. Mol. Biol.* **2015**, *22*, 499−505.
(85) Petkova, A. T.; Ishii, Y.; Balbach, J. J.; Antzutkin, O. N.; Leapman, R. D.; Delaglio, F.; Tycko, R. A structural model for Alzheimer's β-amyloid fibrils based on experimental constraints from solid state NMR. *Proc. Natl. Acad. Sci. U.S.A.* **2002**, *99*, 16742−16747.
(86) Sciarretta, K. L.; Gordon, D. J.; Petkova, A. T.; Tycko, R.; Meredith, S. C. Aβ40-lactam(D23/K28) models a conformation highly favorable for nucleation of amyloid. *Biochemistry* **2005**, *44*, 6003−6014.
(87) Cerofolini, L.; Ravera, E.; Bologna, S.; Wiglenda, T.; Boddrich, A.; Purfurst, B.; Benilova, I.; Korsak, M.; Gallo, G.; Rizzo, D.; Gonnelli, L.; Fragai, M.; De Strooper, B.; Wanker, E. E.; Luchinat, C. Mixing Aβ(1−40) and Aβ(1−42) peptides generates unique amyloid fibrils. *Chem. Commun.* **2020**, *56*, 8830−8833.
(88) Elkins, M. R.; Wang, T.; Nick, M.; Jo, H.; Lemmin, T.; Prusiner, S. B.; DeGrado, W. F.; Stohr, J.; Hong, M. Structural polymorphism of Alzheimer's β-amyloid fibrils as controlled by an E22 switch: A solid-state NMR study. *J. Am. Chem. Soc.* **2016**, *138*, 9840−9852.
(89) Masuda, Y.; Irie, K.; Murakami, K.; Ohigashi, H.; Ohashi, R.; Takegoshi, K.; Shimizu, T.; Shirasawa, T. Verification of the turn at positions 22 and 23 of the β-amyloid fibrils with Italian mutation using solid-state NMR. *Bioorg. Med. Chem.* **2005**, *13*, 6803−6809.
(90) Yamamoto, N.; Hirabayashi, Y.; Amari, M.; Yamaguchi, H.; Romanov, G.; Van Nostrand, W. E.; Yanagisawa, K. Assembly of hereditary amyloid β-protein variants in the presence of favorable gangliosides. *FEBS Lett.* **2005**, *579*, 2185−2190.
(91) Yamamoto, N.; Van Nostrand, W. E.; Yanagisawa, K. Further evidence of local ganglioside-dependent amyloid β-protein assembly in brain. *Neuroreport* **2006**, *17*, 1735−1737.
(92) Kollmer, M.; Close, W.; Funk, L.; Rasmussen, J.; Bsoul, A.; Schierhorn, A.; Schmidt, M.; Sigurdson, C. J.; Jucker, M.; Fandrich, M. Cryo-EM structure and polymorphism of Aβ amyloid fibrils purified from Alzheimer's brain tissue. *Nat. Commun.* **2019**, *10*, 4760.
(93) Tang, T. C.; Hu, Y.; Kienlen-Campard, P.; El Haylani, L.; Decock, M.; Van Hees, J.; Fu, Z.; Octave, J. N.; Constantinescu, S. N.; Smith, S. O. Conformational changes induced by the A21G Flemish mutation in the amyloid precursor protein lead to increased Aβ production. *Structure* **2014**, *22*, 387−396.
(94) Hu, Y.; Kienlen-Campard, P.; Tang, T. C.; Perrin, F.; Opsomer, R.; Decock, M.; Pan, X. S.; Octave, J. N.; Constantinescu, S. N.; Smith, S. O. β-Sheet structure within the extracellular domain of C99 regulates amyloidogenic processing. *Scientific Rep.* **2017**, *7*, 17159.
(95) Hu, Z. W.; Au, D. F.; Cruceta, L.; Vugmeyster, L.; Qiang, W. N-Terminal modified Aβ variants enable modulations to the structures and cytotoxicity levels of wild-type Aβ fibrils through cross-seeding. *ACS Chem. Neurosci.* **2020**, *11*, 2058−2065.
(96) Bakrania, P.; Hall, G.; Bouter, Y.; Bouter, C.; Beindorff, N.; Cowan, R.; Davies, S.; Price, J.; Mpamhanga, C.; Love, E.; Matthews, D.; Carr, M. D.; Bayer, T. A. Discovery of a novel pseudo β-hairpin structure of N-truncated amyloid-β for use as a vaccine against Alzheimer's disease. *Mol. Psychiatry* **2021**, DOI: 10.1038/s41380-021-01385-7.
(97) Arndt, J. W.; Qian, F.; Smith, B. A.; Quan, C.; Kilambi, K. P.; Bush, M. W.; Walz, T.; Pepinsky, R. B.; Bussiere, T.; Hamann, S.; Cameron, T. O.; Weinreb, P. H. Structural and kinetic basis for the selectivity of aducanumab for aggregated forms of amyloid-beta. *Scientific Rep.* **2018**, *8*, 6412.
(98) Seuma, M.; Faure, A. J.; Badia, M.; Lehner, B.; Bolognesi, B. The genetic landscape for amyloid β fibril nucleation accurately discriminates familial Alzheimer's disease mutations. *eLife* **2021**, *10*, e63364 DOI: 10.7554/eLife.63364.